HEAT BUDGET PARAMETERIZATION FOR THE FNWC PRIMITIVE EQUATION MODEL USING DATA FOR 16 OCTOBER 1973

Michael Dennis Warner

NAVAL POSTGRADUATE SCHOOL
Monterey, California

THESIS

HEAT BUDGET PARAMETERIZATION
FOR THE FNWC PRIMITIVE EQUATION
MODEL USING DATA FOR 16 OCTOBER 1973

by

Michael Dennis Warner

September 1974

Thesis Advisor: F. L. Martin

SECURITY CLASSIFICATION OF THIS PAGE *(When Data Entered)*

REPORT DOCUMENTATION PAGE

READ INSTRUCTIONS BEFORE COMPLETING FORM

1. REPORT NUMBER	2. GOVT ACCESSION NO. / 3. RECIPIENT'S CATALOG NUMBER
4. TITLE *(and Subtitle)*: HEAT BUDGET PARAMETERIZATION FOR THE FNWC PRIMITIVE EQUATION MODEL USING DATA FOR 16 OCTOBER 1973	5. TYPE OF REPORT & PERIOD COVERED: Master's Thesis' September 1974
	6. PERFORMING ORG. REPORT NUMBER
7. AUTHOR(s): Michael Dennis Warner	8. CONTRACT OR GRANT NUMBER(s)
9. PERFORMING ORGANIZATION NAME AND ADDRESS: Naval Postgraduate School, Monterey, California 93940	10. PROGRAM ELEMENT, PROJECT, TASK AREA & WORK UNIT NUMBERS
11. CONTROLLING OFFICE NAME AND ADDRESS: Naval Postgraduate School, Monterey, California 93940	12. REPORT DATE: September 1974
	13. NUMBER OF PAGES: 105
14. MONITORING AGENCY NAME & ADDRESS *(if different from Controlling Office)*: Naval Postgraduate School, Monterey, California 93940	15. SECURITY CLASS. *(of this report)*: Unclassified
	15a. DECLASSIFICATION/DOWNGRADING SCHEDULE

16. DISTRIBUTION STATEMENT *(of this Report)*

Approved for public release; distribution unlimited.

17. DISTRIBUTION STATEMENT *(of the abstract entered in Block 20, if different from Report)*

18. SUPPLEMENTARY NOTES

19. KEY WORDS *(Continue on reverse side if necessary and identify by block number)*

Tropospheric Heat Balance Model; Radiation Budget; Cloud Parameterization

20. ABSTRACT *(Continue on reverse side if necessary and identify by block number)*

This study was an evaluation of a two-cloud layer heating model for inclusion in a numerical weather prediction model over the ice-free ocean. The model employs empirical formulations for atmospheric absorptivities, scattering, and reflectivity, and cloud and earth surface reflectivity to compute solar insolation received and absorbed at earth and in the key tropospheric layers above. Long-wave emissivity

DD FORM 1 JAN 73 1473 EDITION OF 1 NOV 65 IS OBSOLETE
S/N 0102-014-6601 |
(Page 1)

SECURITY CLASSIFICATION OF THIS PAGE *(When Data Entered)*

Block 20 - ABSTRACT (Cont.)

formulas by Sasamori for water-vapor and carbon dioxide are computed to determine cooling by the earth and troposphere. To complete the heat budget scheme for the earth's surface and near surface boundary layer, vertical transport of sensible and latent heat at the surface was evaluated.

To check the validity of this model, both instantaneous heating rates and 24-hour averaged rates were computed for the earth-atmosphere system, the atmospheric column and the earth's surface using data in the form of gridpoint soundings over the Atlantic and Pacific Oceans for 15-16 October 1973, provided by Fleet Numerical Weather Central.

Heat Budget Parameterization for the FNWC Primitive Equation Model Using Data for 16 October 1973

by

Michael Dennis Warner
Lieutenant, United States Navy
B.S., Baylor University, 1966

Submitted in partial fulfillment of the
requirements for the degree of

MASTER OF SCIENCE IN METEOROLOGY

from the

NAVAL POSTGRADUATE SCHOOL
September 1974

ABSTRACT

This study was an evaluation of a two-cloud layer heating model for inclusion in a numerical weather prediction model over the ice-free ocean. The model employs empirical formulations for atmospheric absorptivities, scattering, and reflectivity, and cloud and earth surface reflectivity to compute solar insolation received and absorbed at earth and in the key tropospheric layers above. Long-wave emissivity formulas by Sasamori for water-vapor and carbon dioxide are computed to determine cooling by the earth and troposphere. To complete the heat budget scheme for the earth's surface and near surface boundary layer, vertical transport of sensible and latent heat at the surface was evaluated.

To check the validity of this model, both instantaneous heating rates and 24-hour averaged rates were computed for the earth-atmosphere system, the atmospheric column and the earth's surface using data in the form of grid point soundings over the Atlantic and Pacific Oceans for 15-16 October 1973, provided by Fleet Numerical Weather Central.

TABLE OF CONTENTS

LIST OF TABLES

LIST OF FIGURES

Figure

LIST OF SYMBOLS

A(m,n) - solar insolation absorbed in the layer (m,n)

$\bar{a}(m,n)$ - Manabe-Möller absorptivity function

a* - turbulent transfer coefficient

ABA - absorptivity of the troposphere

ABG - total insolation absorbed by earth's surface

ALB - earth-atmospheric system albedo

ATRAN - transmissivity of the troposphere

B_k - Stefan-Boltzmann blackbody flux at T_k

BALB - 24-hour averaged radiational balance at earth's surface

$BALk_1k_2$ - 24-hour averaged radiational balance for layer (k_1,k_2)

BALT - 24-hour averaged radiational balance at tropopause

C - carbon dioxide layer absorber mass

CL - total opaque cloud cover

CL(I) - fractional cloud amount for layer: I=1 in 600 to 400 mb; I=2 in 900 to 800 mb

E - East longitude; evaporation

e_x - vapor pressure at top of constant flux layer

F(A) - solar insolation subject to water vapor absorption only

FADJ - total incoming insolation at top of atmosphere

Fk_1k_2 - net infrared flux divergence between level k_1 and k_2

F_k* - net infrared flux at level k

FNWC - Fleet Numerical Weather Central

F(S) - solar insolation subject to Rayleigh scattering only

g - gravity

h - hour angle

H - height of homogeneous atmosphere; 24-hour averaged hour angle

H_Γ - sensible heat transport

I - abscissa grid location

IA10(m,n) - solar insolation absorbed at surface with cloud condition (m,n)

IS10(m,n) - solar insolation at surface subject to Rayleigh scatter with cloud condition (m,n)

J - ordinate grid location

k - pressure level used in this study equal to 10σ

K* - eddy turbulent transfer coefficient

L - latent heat of vaporization

M - water-vapor mass path length

N - North latitude

P_k - pressure in millibars (mb) at level k

q_k - mixing ratio at level k

q_{s_k} - saturated mixing ratio at level k

QAVE - 24-hour averaged insolation at the tropopause

r - Bowen ratio

R - correlation coefficient; net radiation balance at the surface

R_a - mean radiative cooling rate in troposphere

R_d - universal gas constant

REF - total insolation reflected back to space

REFA - F(A) insolation reflected back to space

REFS - F(S) insolation reflected back to space

R.H. - relative humidity

R_s - mean radiative energy gain (loss) rate at ocean-troposphere system

S - South latitude; effective solar constant; heat storage at surface

S_a - heat storage term for the troposphere

T_k - temperature at level k

TRAN - total insolation incident at the earth's surface

T_x - temperature at the top of constant flux layer

U - water-vapor layer absorber mass

W - West latitude

W(m,n) - cloud fractional weight for cloud condition (m,n)

Z - Zenith angle

Z_k - height at level k

$\alpha(G)$ - surface albedo

$\alpha(R)$ - Rayleigh clear sky albedo

γ_c - critical lapse rate

δ - solar declination angle

ε_{wc} - emissivity due to water and carbon dioxide absorber mass at indicated layer

θ_k - potential temperature at level k

Λ - longitude

π - surface pressure; pi = 3.1416

ρ - density

σ - sigma pressure level used by FNWC, normalized to surface pressure

ϕ - latitude

ACKNOWLEDGEMENT.

The author wishes to express his appreciation to his thesis advisor, Professor F. L. Martin, for his suggestions, advice, guidance and support in this research and to Mr. Russel D. Schwanz for his expert programming assistance.

Appreciation is also expressed to the author's wife for her support and perseverance and to Mrs. Donna Grigsby for typing this manuscript.

I. INTRODUCTION

This study was part of an ongoing project to produce an empirical heat budget parameterization for utilization in the Fleet Numerical Weather Central (FNWC) primitive equation prediction model. The project will eventually examine the heat balance of the earth-ocean system using representative mid-seasonal data from each of the four seasons of the year 1973-74. This particular study covers 15-16 October 1973, using gridded FNWC temperature and humidity fields, at constant pressure levels, for this period.

The parameters which influence the radiative calculations most strongly are the two cloud layers of fractional amounts CL(1) and CL(2), at 600 and 900 mb, respectively, at each grid point. The fractional amounts are specified using the large-scale formulations developed by Smagorinsky (1960) as also was done by Jenks (1974). The possibility of two cloud layers introduces substantial complexity to the radiative physics compared to the one-layer cloud model previously described by Martin (1972). The adaptation of the radiational model to FNWC gridpoint soundings is based on an unpublished manuscript (Martin, 1974). The Martin manuscript in turn has similarities to the multi-cloud heating packages of Arakawa (1972) and Rodgers (1967).

Heat-balance computations were made at the ocean surface, at the tropopause, and for the atmospheric layer surface to

200 mb. A major purpose was to determine whether the cloud-cover parameterization previously adopted by Jenks (1974) lends itself to realistic budgetary computations (as compared to the results of others) for Oct. 15-16 over the Northern Hemispheric oceans. In studying the net heating effects at the ocean surface, the evaporative and sensible-heat transfers were modeled after Kesel and Winninghoff (1972), and Kaitala (1974), but with some modifications to be described later (Section V).

To assess the effects of the cloud cover parameterization on the heat transfers of this study, gridpoint data along four meridians were selected from the FNWC analyses of 15-16 October 1973. Three of the meridians are from the Pacific Ocean area and the fourth is from the Atlantic Ocean (see Fig. 2). Most of the gridpoint soundings sampled were in the Northern Hemisphere.

The five sigma ($\sigma = p/\pi$) analysis levels of the FNWC primitive equation model were adapted for data input in the vertical scale of this study. The k-levels (k=1,...,10), where $k=10\sigma$, are used for the purpose of simplified referencing of the data levels in the equations derived and are shown in Fig. 1. The cloud layers, when they exist, are considered to be in two layers, a high-level cloud layer from k=4 to k=6 and a low-level cloud deck from k=8 to k=9, with amounts CL(1) and CL(2), respectively. In pressure-scaling the water vapor and CO_2 absorber masses a realistic method, after Smith (1966), was used to extrapolate water vapor

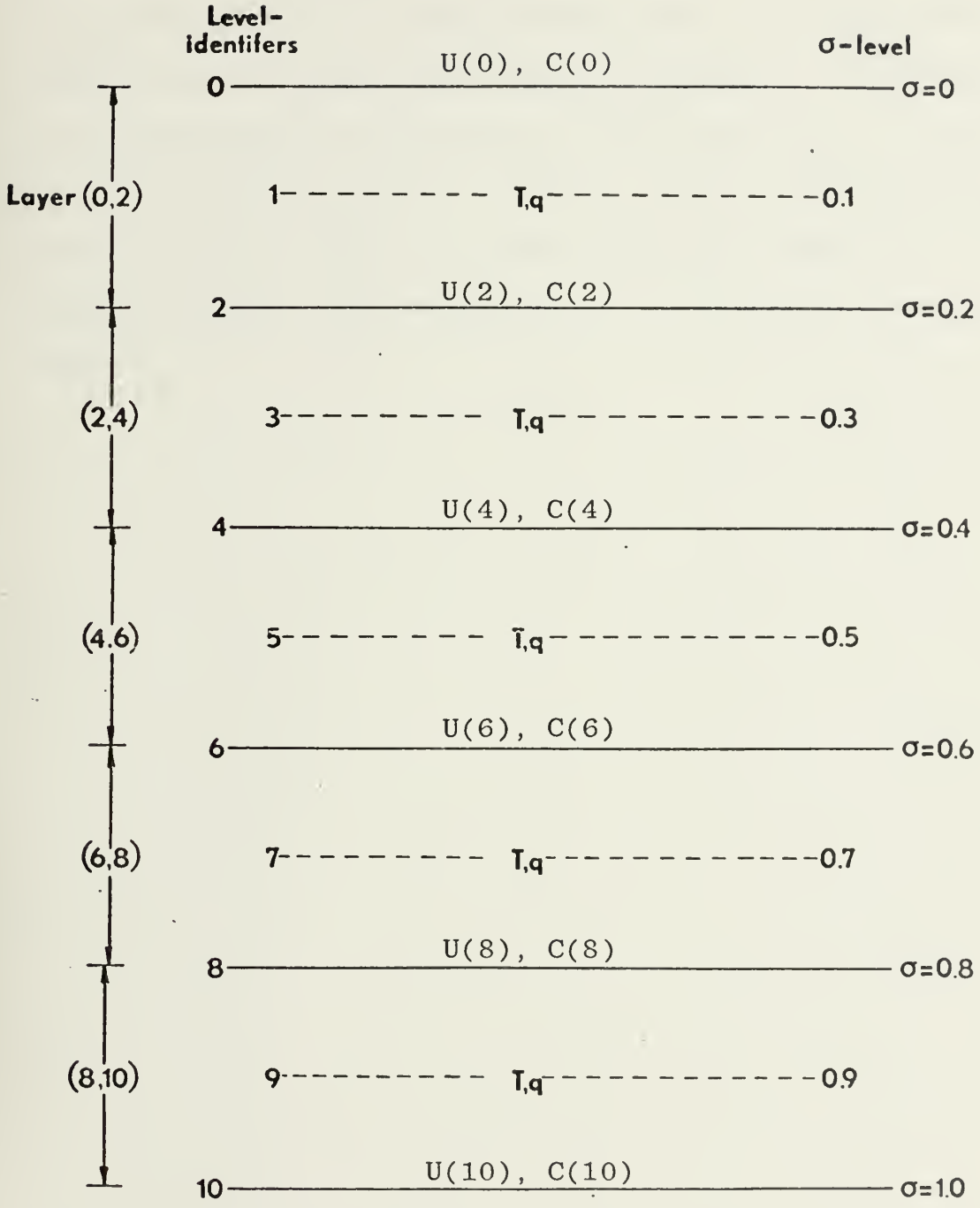

Figure 1. Five-layer radiative sounding used in this study. Levels are identified by their values on the k-scale, while layers are identified by their level boundary indices in parentheses, e.g. (8,10). Pressure-scaled water vapor and CO_2 mass increments U and C, respectively, are integrated with respect to the surface and introduced at even levels while the mixing ratio, q, is formulated at odd levels. The temperature, T, is expressed for all levels.

mixing ratio values above the level of k=4, where radiosonde moisture data is normally not available. The net flux of terrestrial radiation computations make use of empirical absorptivities of water vapor and CO_2 (Sasamori, 1968), which are incorporated in the Martin (1974) manuscript. The solar radiation package in Martin (1974) has been modeled after Arakawa (1972), except that only two cloud layers are considered possible, as contrasted with three in the Arakawa version.

II. DATA PREPARATION

The data used in this study was in the form of gridpoint soundings chosen along four meridians of FNWC 63-by-63 grid-mesh temperature and humidity data fields to insure minimum over land data. The three meridians (and their respective number of soundings) selected over the Pacific Ocean were located at 125°W - (25 soundings), 170°W - (25 soundings), and 145°E - (17 soundings). The Atlantic Ocean meridian was 35°W - (26 soundings). Fig. 2 shows how the meridians were located on the FNWC polar stereographic grid. This procedure of choosing data lines along diagonals or along J=32 (through the pole-point) of the FNWC data-fields obviates the necessity of interpolating spatially to gridpoints. Data along line 3 in the Pacific were not extended southward of (9,55) because they fell over land masses (New Guinea and Northern Australia) where the surface temperatures were too high to be representative of the oceanic values.

The vertical soundings on these data lines were taken from the original FNWC 63-by-63 gridpoint analysis of temperature at the surface and at nine other standard levels up to 100 millibars for 0000GMT, 16 October 1973 for the Pacific Ocean data cases and 12 hours earlier for the Atlantic Ocean data cases. In addition to these standard level values, a T_x value was listed which is the FNWC calculated temperature (see Kesel and Winninghoff, 1972) for the top of the turbulent layer of constant sensible heat flux. This level,

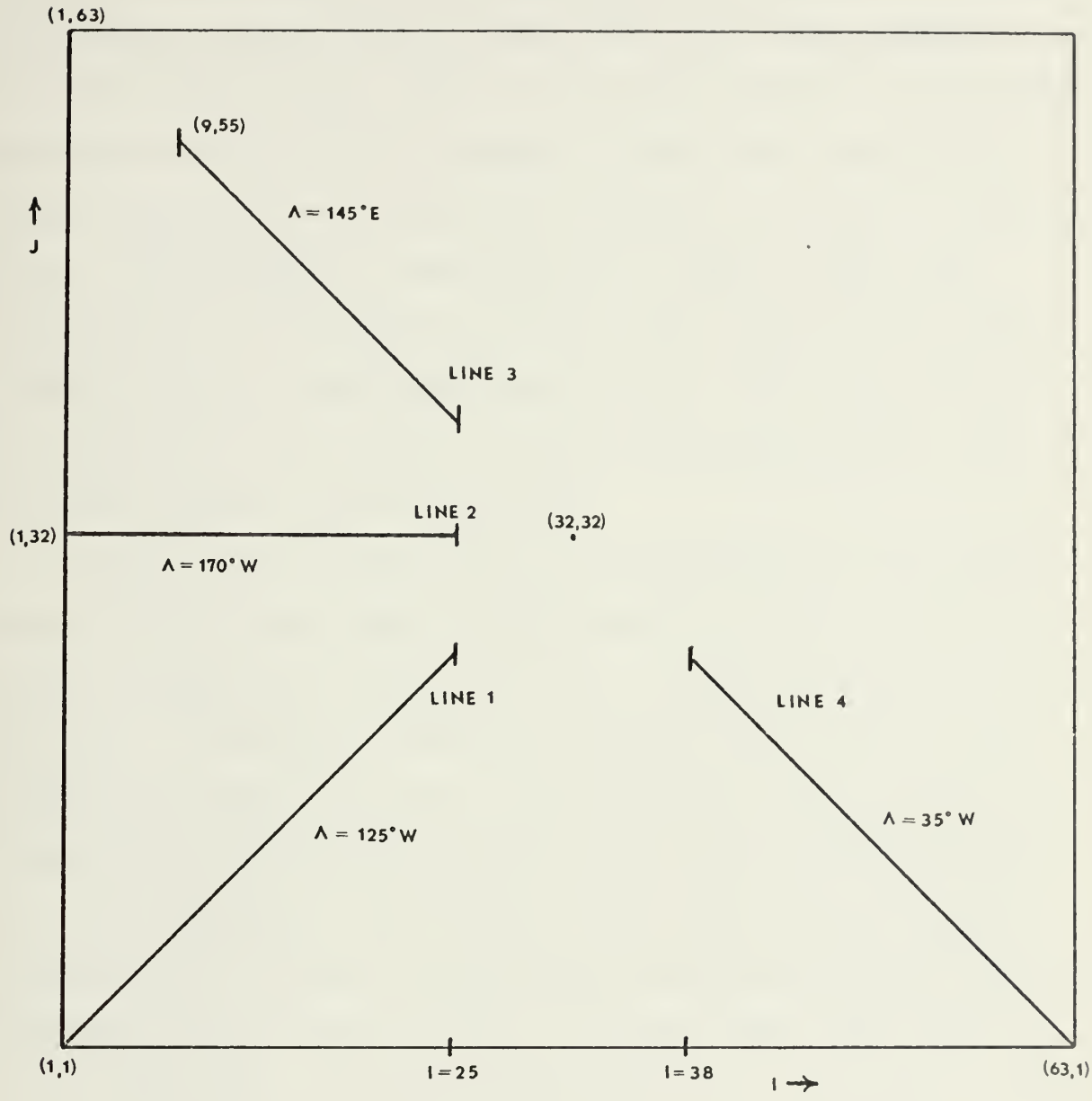

Figure 2. FNWC polar stereographic grid and meridians (lines 1, 2, 3, and 4) selected for study. The longitudes Λ are shown for each meridian as well as the extent considered of each meridian.

which is approximately 20 meters above the surface, was designated by a code label of 9999 under the column labeled pressure (Table I(a)). The six moisture values of this table were given by the vapor pressure at sea level, and by dew-point depression for levels from 925 mb to 400 mb. In addition, the parameter e_x was provided by FNWC as the vapor pressure at the top of the constant flux layer at the level indicated by the code 9999 (Table I(a)). Table I(a) gives an example of the original sounding for gridpoint (1,1) of the FNWC map for the given period.

In order to perform radiative calculations, it is necessary to have water vapor and CO_2 absorber masses and cloud amounts within the required k-level boundaries (Fig. 1). To do this, a systematic method was applied to arrive at the temperature and mixing ratio distributions (Table I(b)) as detailed in the following subsections. It should be noted that all soundings start at sea level, but as a reasonable approximation surface pressure was considered to be $\pi \simeq 1000$ mb. Therefore the k-levels of Fig. 1 become 1000., 900., 800., ..., 200., 100., 0.0 mb, respectively.

Table I(a). Example of an original FNWC gridpoint sounding for point (1,1). The humidity parameters for the surface and the tope of the constant flux layer (9999) are vapor pressures and those between 925,...,400 mb are dew-point depression.

Pressure (mb)	T(°C)	Humidity Parameters
surface	25.5	25.6 mb
925	19.3	3.6°C
850	15.5	3.2°C
700	6.5	5.4°C
500	-10.2	5.4°C
400	-21.9	2.1°C
300	-36.8	
250	-45.8	
200	-56.0	
150	-67.3	
100	-80.6	
9999*	T_x = 24.7	e_x = 26.3 mb

Table I(b). Example of the corresponding radiative sounding with temperature and mixing ratio listed at k-levels.

Pressure (mb)	T(°K)	Mixing Ratio (g/kg)
1000	298.7	15.92
900	290.9	11.45
800	285.9	
700	279.7	5.95
600	272.4	
500	263.0	2.31
400	251.3	1.42
300	236.4	0.56
200	217.2	
100	192.6	0.03
0	192.6	0.00

* Values at top of constant flux layer as used in FNWC heating package (Kesel and Winninghoff, 1972).

A. TEMPERATURE TERMS

The temperatures were listed at each mandatory level between the surface and 100 mb. The temperature T_{10} was set equal to the listed surface air temperature. At the top of the atmosphere, the temperature was assumed to be isothermal from 100 mb to P=0 mb, with the mixing ratio approaching zero at P=0 mb. The radiative sounding temperatures for the remaining k-levels were obtained from either their corresponding listed temperature or by a three-point Lagrangian interpolation scheme of the form:

$$\begin{aligned} T_k = {} & T_0((P_k-P_1)(P_k-P_2))/((P_0-P_1)(P_0-P_1)) \\ & + T_1((P_k-P_0)(P_k-P_2))/((P_1-P_0)(P_1-P_2)) \\ & + T_2((P_k-P_0)(P_k-P_1))/((P_2-P_0)(P_2-P_1)) \end{aligned} \qquad (2\text{-}1)$$

Here k is the pressure level desired for T_k interpolation, P_0 lies above P_k, and P_1, P_2 lie below level k. The parameters T_0, T_1, and T_2 are temperatures at the same levels as P_0, P_1 and P_2, respectively. As an example, if k=9, P_1 and P_2 were taken as 925 mb and 1000 mb, respectively.

The T_x temperature was not utilized in the interpolation scheme described above, but was carried along as a twelfth temperature for later use in the heat budget computations.

B. MOISTURE TREATMENT IN THE SOUNDING

The moisture parameters from the original FNWC soundings (Table I(a)) were converted into mixing ratios at each of the original sounding levels. At k=10 the surface vapor pressure, e_{air}, was used to calculate the mixing ratio as

follows:

$$q_{1000} \simeq .62197\ e_{air}/1000 \qquad (2\text{-}2)$$

where e_{air} is in millibars. To obtain a mixing ratio for the top of the constant flux layer, Equation (2-3) was used to compute q_x from e_x

$$q_x \simeq (e_x/1000)\ .62197 \qquad (2\text{-}3)$$

where e_x is the vapor pressure at the top of the constant flux layer in mb.

The mixing ratio at level P is calculated at the remaining original data levels by the use of Equation (2-4) which is taken from Fleagle and Businger (p. 63, 1963);

$$q(P) = \frac{621.97\ e^{(A-B/T)}}{P} \exp\left[\frac{-B(T-T_D)}{TT_D}\right] \qquad (2\text{-}4)$$

A = 21.656

B = 5418.0°K

T = temperature °K at level P

T_D = dew point (°K) at level P

The calculated q-values were then interpolated to the k-levels using an equation similar to Equation (2-1). An example of the interpolation results for gridpoint (1,1) is shown in Table I(b).

Since accurate humidity information is not generally available for the upper troposphere, a logarithmic extrapolation formula was used to find q-values at k=1, 2, and 3.

$$\frac{q(P)}{q_5} = \left(\frac{P}{500}\right)^{\lambda} \qquad (2\text{-}5)$$

This formula as described by Jenks (1974) is similar to that developed by Smith (1966). It is solved, using a "best-fit" between variables $y \equiv \log \frac{q}{q_5}$ and $x \equiv \log \frac{P}{500}$, for the parameter λ. The six q-values of the original soundings corresponding to P = 1000, 925, 850, 700, 500, and 400 mb are used to determine λ, which is then used in Equation (2-5) to extrapolate the q values to P = 300, 200, and 100 mb.

A correlation coefficient was statistically computed in connection with each λ-profile of the form:

$$R_{y/x} \equiv \lambda \sqrt{\frac{\sum_{i=1}^{6} x_i^2}{\sum_{i=1}^{6} y_i^2}}$$

The correlation coefficient enabled the monitoring of the usefulness of the λ-profile technique and was generally found to be in the range of 0.95 to 0.99.

C. PRESSURE-SCALED ABSORBER MASSES

Having computed the mixing ratios at each odd k-level, it is now possible to compute the pressure-scaled water vapor absorber masses in each layer. In Figure 1, these water vapor layer-masses were denoted by U, however here we will use notation which is more representative of the particular layer under consideration. For example, the pressure-scaled water vapor mass in the lowest layer (8,10) is given by

$$U(8,10) = \frac{q_9 \Delta P}{g} \left[\frac{P_9}{1013.25}\right]^{0.72} \qquad (2\text{-}6)$$

where the Möller and Raschke (1964) pressure-scaling exponent 0.72 has been employed. For the layer (6,8), an analog to Equation (2-6) was used by replacing the parameters with the subscript 9 with their counterpart parameters with the subscript 7. A similar procedure was followed for the remaining layers (4,6), (2,4), (0,2). In each of the five layers ΔP = 200 mb.

The algorithm for computing the integrated water vapor mass above the earth's surface is as follows:

$$\begin{aligned} U(10) &= 0.0 \\ U(8) &= U(10) + U(8,10) \\ U(6) &= U(8) + U(6,8) \\ U(4) &= U(6) + U(4,6) \\ U(2) &= U(4) + U(2,4) \\ U(1) &= U(2) + 0.5U(0,2) \\ U(0) &= U(2) + U(0,2) \end{aligned} \qquad (2\text{-}7)$$

A similar computation scheme is used for the carbon dioxide scaled mass. Here, however it is customary to represent the pressure-scaled mass in terms of the normal temperature and pressure (N.T.P.) volume over a cm^2 of the earth's surface. Thus for the lower layer:

$$C(8,10) = 3.14 \times 10^{-4}\left(\frac{\Delta P}{g\rho_s}\right)\left(\frac{P_9}{1013.25}\right)^{0.72} \qquad (2\text{-}8)$$

The fractional amount 3.14×10^{-4} is the constant mixing ratio of CO_2 by volume, and $\frac{\Delta P}{g\rho_s}$ is the N.T.P. thickness of the layer $\Delta P = P_{10}-P_8$. The quantity ρ_s is constant density in a standard homogeneous atmosphere of depth H where T_s=273.16°K

everywhere and P_s = 1013.25 mb. The parameter H, also generally known as the scale height of the homogeneous atmosphere, may be further defined as:

$$H = \frac{RT_s}{g} = 7.995 \times 10^5 \text{ cm}$$

Therefore Equation (2-8) may be rewritten as

$$C(8,10) = 3.14 \times 10^{-4} H\left(\frac{\Delta P}{1013.25}\right)\left(\frac{P_9}{1013.25}\right)^{0.72} \qquad (2\text{-}9)$$

All other layer thicknesses of CO_2 are obtained in a similar manner to Equation (2-9) by substituting the appropriate subscripted indices 7,5,...,1 on the pressure P.

The algorithm for computing the integrated carbon dioxide mass above the earth's surface is as follows:

$$\begin{aligned} C(10) &= 0.0 \\ C(8) &= C(10) + C(8,10) \\ C(6) &= C(8) + C(6,8) \\ C(4) &= C(6) + C(4,6) \\ C(2) &= C(4) + C(2,4) \\ C(1) &= C(2) + 0.5C(0,2) \\ C(0) &= C(2) + C(0,2) \end{aligned} \qquad (2\text{-}10)$$

D. CLOUD PARAMETERIZATION

In order to determine the fractional cloud cover amounts in the layers (4,6) and (8,9), the saturated vapor pressure must be calculated at levels k=5 and k=9, respectively by the following equations:

$$q_S(500) = \frac{.62197\ e^{(A-B/T_5)}}{500} \qquad (2\text{-}11a)$$

$$q_S(900) = \frac{.62197\ e^{(A-B/T_9)}}{900} \qquad (2\text{-}11b)$$

where A = 21.656 and B = 5418.0°K as before in Eq. (2-4).

Knowing the saturated vapor pressure at levels k=5 and k=9 enables the determination of the relative humidity at those levels:

$$R.H.(5) = \frac{q(500)}{q_S(500)} \qquad (2\text{-}12a)$$

$$R.H.(9) = \frac{q(900)}{q_S(900)} \qquad (2\text{-}12b)$$

The relative humidities were then substituted into Smagorinsky's (1960) formulation for fractional cloud amounts:

$$CL(1) = 2.0\ (RH(5)) - 0.7 \qquad (2\text{-}13a)$$

$$CL(2) = 3.33\ (RH(9)) - 2.0 \qquad (2\text{-}13b)$$

These formulations were employed by Jenks (1974) and are also to be tested in this study in which a different seasonal sample is considered.

These fractional cloud amounts are a function of large scale influences only and do not consider small scale convective activity, seasonal conditions or latitude. The use of such clouds is for radiational study only.

III. TERRESTRIAL RADIATION

A. THEORETICAL AND EMPIRICAL BASIS

Empirical formulas were developed by Sasamori (1968) for computing emissivities for long-wave flux calculations associated with the NCAR General Circulation Model. These empirical emissivity formulas can be related to the values built into Yamamoto's (1952) well known Radiation Chart, which was developed from radiative transfer theory. This chart has proved to be very accurate for computational purposes, and was used by Jenks (1974) as a schematic guide for integration of the radiative transfers through the various layers of interest in the soundings discussed in Section II.

The necessary emissivity formulas of Sasamori for utilization in the FNWC heating package are those which will yield expressions for:

F_{10}* = Net IR flux at earth surface

F_6* = Net IR flux at level k=6

F_2* = Net IR flux at level k=2

F610 = Net IR flux divergence in the layer (6,10)

F26 = Net IR flux divergence in the layer (2,6)

A workable scheme for making these computations is presented below for various combinations of cloud cover [CL(1), CL(2)]. For example, in order to compute

$$F_{10}^* = B_{10} - \int_{B=0}^{B_{10}} \varepsilon_{wc}(U,C,T)dB \qquad (3\text{-}1)$$

where B_k is the Stefan-Boltzmann blackbody flux at T_k, one must have a good representation of the emissivity ε_{wc} as a function of both water vapor and carbon dioxide absorber masses (U and C, respectively) along the sounding which is the path of integration. For the integral evaluation of Eq. (3-1), Sasamori (1968) proposed temperature-independent emissivity formulations ε_{wc} as exemplified for the absorber masses in layer (8,10) as follows:

$$\varepsilon_{wc}(8,10) = \{.240 \log_{10}[U(8,10)]+.622\}+.07262\{(1. -.62556[U(8,10)+.0286]^{\cdot 26})[\log_{10}C(8,10) +1.064]\} \qquad (3\text{-}2)$$

Formulas of the type given by Eq. (3-2) apply for $T \geq 210°K$. The quantity in the first brace of Eq. (3-2) indicates the water vapor emissivity alone and that in the second brace is the additional contribution by that part of the CO_2 emissivity not already included in the water vapor emissivity expression.

Eq. (3-2) was used in the calculation of the atmospheric emissivities over all layers (6,10), (4,10),....,(1,10), for which cumulative mass values U(6,10), C(6,10), etc., were available from the radiative soundings. Thus Eq. (3-2) proved very versatile. For completion of the integration from level k=1 to the origin (B=0, ε=1.0) of Yamamoto's Radiation Chart, the $U(T_k)$, $C(T_k)$ soundings were taken to be isothermal at $T=T_1$ to the top of atmosphere (to level "0"). This leaves only the temperature-dependent emissivity $\tilde{\varepsilon}_{wc}$

$[U(0,10),T_1]$ which applied for $T \leq 210°K$, also computed after Sasamori (1968) by means of

$$\tilde{\varepsilon}_{wc}\,U(0,10),T_1 = 8.34T_1^{[.353\,\log_{10}U(0,10)-.44]} \times U(0,10)^{[-.03455\,\log_{10}U(0,10)-.705]} \times [8.0/(.353\,\log_{10}U(0,10)+3.56)] + .07262\{(1.-.62556[U(0,10)+.0286]^{.26}) \times [\log_{10}C(0,10)+1.064]\} \qquad (3\text{-}3)$$

The first term is temperature-dependent, as well as dependent upon the summed absorber masses relative to the reference level (in this example, level k=10). The term in the brace involves essentially the same form of the CO_2 correction to the total emissivity as seen in Eq. (3-2) except that it refers to the full layer (0,10). Eq. (3-3) is applicable with appropriate final parameters U(0,k), C(0,k), and T_1 to the determination of the downward flux contributions through level k for all of the reference level cases to be considered below, i.e. k=2,6,10.

B. NET FLUX F_{10}*

The radiative soundings were evaluated in the form of the parameters U(k,10), C(k,10), and T_k, level by level. Also listed for each radiative sounding are the cloud cover parameters CL(1) and CL(2), which in general are non-zero. The grid area may be visualized as composed of areal fractions or weights defined as follows:

$W(0,0) = (1-CL(1))(1-CL(2))$: totally clear fraction

$W(1,0) = (CL(1))(1-CL(2))$: overcast in upper layer only

$W(0,1) = (1-CL(1))(CL(2))$: overcast in lower layer only (3-4)

$W(1,1) = (CL(1))(CL(2))$: overcast in both layers

The composite radiative effect of the true cloud cover over the grid area is then reconstructed by multiplying the results of the respective cases defined above by the appropriate weight factors. The four cases will now be defined in order.

1. Net Flux F_{10}* with Clear Skies

Defining the Stefan-Boltzmann blackbody flux at T_k as B_k, where $B_k = 1.170403 \times 10^{-7}\ T_k^4$ ly(day)$^{-1}$, the net flux at the surface under the clear sky case is defined as follows:

$$\begin{aligned} F_{10}^*(0,0) = B_{10} - .5\{&\varepsilon_{wc}(8,10)(B_{10}-B_8)+(B_8-B_6)[\varepsilon_{wc}(6,10) \\ &+\varepsilon_{wc}(8,10)]+[\varepsilon_{wc}(4,10)+\varepsilon_{wc}(6,10)](B_6-B_4) \\ &+(B_4-B_2)[\varepsilon_{wc}(2,10)+\varepsilon_{wc}(4,10)]+[\varepsilon_{wc}(1,10) \\ &+\varepsilon_{wc}(2,10)](B_2-B_1)+\tilde{\varepsilon}_{wc}[(0,10),T_1]B_1\} \end{aligned} \quad (3\text{-}5)$$

2. Net Flux F_{10}* with Overcast Clouds in Upper Layer Only (k=4 to k=6)

$$\begin{aligned} F_{10}^*(1,0) = (B_{10}-B_6)\{1.-.5[&\varepsilon_{wc}(8,10)(B_{10}-B_8) \\ &+(\varepsilon_{wc}(8,10)+\varepsilon_{wc}(6,10))(B_8-B_6)]\} \end{aligned} \quad (3\text{-}6)$$

3. Net Flux F_{10}* with Overcast in Lower Layer Only (k=8 to k=9)

$$F_{10}^*(0,1) = (B_{10}-B_9)[1.-.5\varepsilon_{wc}(9,10)] \qquad (3\text{-}7)$$

4. Net Flux F_{10}* with Overcast Clouds in Both Layers (4,6) and (8,9)

$$F_{10}^*(1,1) = (B_{10}-B_9)[1.-.5\varepsilon_{wc}(9,10)] \qquad (3\text{-}8)$$

It should be noted that Eq. (3-7) and Eq. (3-8) are identical.

5. Composite F_{10}* Calculations

The composite results are obtained by multiplying the above defined four cases by their respective weights as defined by Eq. (3-4) to obtain

$$\begin{aligned} F_{10}^* = {} & [1-CL(2)]\{(B_{10}-B_6)-.5\varepsilon_{wc}(8,10)(B_{10}-B_8) \\ & +[\varepsilon_{wc}(8,10)+\varepsilon_{wc}(6,10)](B_8-B_6)\} \\ & +(1-CL(2))(1-CL(1))\{B_6-.5[(\varepsilon_{wc}(6,10) \\ & +\varepsilon_{wc}(4,10))(B_6-B_4)+(\varepsilon_{wc}(4,10)+\varepsilon_{wc}(2,10))(B_4-B_2) \\ & +(\varepsilon_{wc}(2,10)+\varepsilon_{wc}(1,0))(B_2-B_1)+\tilde{\varepsilon}_{wc}((0,10),T_1)B_1]\} \\ & +CL(2)\{(B_{10}-B_9)[1-.5\varepsilon_{wc}(9,10)]\} \end{aligned} \qquad (3\text{-}9)$$

It is clear that Eq. (3-9) reduces to F_{10}*(0,0) when CL(1) = CL(2) = 0, and to F_{10}*(1,1) when CL(1) = CL(2) = 1.0. In a similar manner the other two cloud cases may be recovered by setting the weights to CL(1) = 1.0, CL(2) = 0 and CL(2) = 1.0, CL(1) = 0, respectively.

The above described procedure for obtaining the net flux can similarly be extended to levels k=6 and k=2 as listed in the following subsections.

The composite F_{10}* values will be compared in Section III.F with climatology (Malkus, 1962) to ensure the reasonableness of this calculation.

C. NET FLUX F_6*

The individual cases for F_6* can be obtained from the composite F_6* as described above for F_{10}*. The numerical from using the Sasamori type emissivities [Eqs. (3-2) and (3-3)] for the composite F_6* is as follows:

$$F_6^* = [1-CL(1)]\{B_8-.5[\varepsilon_{wc}(6,8)(B_8-B_6)+\varepsilon_{wc}(4,6)(B_6-B_4)$$
$$+(\varepsilon_{wc}(4,6)+\varepsilon_{wc}(2,6))(B_4-B_2)+(\varepsilon_{wc}(2,6)+\varepsilon_{wc}(1,6))(B_2-B_1)$$
$$+\tilde{\varepsilon}_{wc}((0,6),T_1)B_1]\}+(1-CL(1))(1-CL(2))\{(B_{10}-B_8)[1.$$
$$-.5(\varepsilon_{wc}(6,8)+\varepsilon_{wc}(6,10))]\}+CL(1)\{(B_8-B_6)[1-.5(\varepsilon_{wc}(6,8))]\}$$
$$+CL(1)(1-CL(2))\{(B_{10}-B_8)[1-.5(\varepsilon_{wc}(6,8)+\varepsilon_{wc}(6,10))]\} \quad (3\text{-}10)$$

D. NET FLUX F_2*

In a similar fashion to F_{10}* and F_6* the net flux at level k=2 can be calculated from the radiation chart using the trapezoidal rule as described by Jenks (1974). Again the numerical formulation of the individual cloud cases can be obtained from the composite net flux formula as described in Subsection III.B.5. The composite F_2* formula is

$$F_2^* = [1-CL(1)]\{B_8-.5[\varepsilon_{wc}(2,4)(B_4-B_2)+(\varepsilon_{wc}(2,4)$$
$$+\varepsilon_{wc}(2,6))(B_6-B_4)+(\varepsilon_{wc}(2,6)+\varepsilon_{wc}(2,8))(B_8-B_6)$$
$$+\varepsilon_{wc}(1,2)(B_2-B_1)+\tilde{\varepsilon}_{wc}((0,2),T_1)B_1]\}+(1-CL(1))(1-CL(2)) \quad (3\text{-}11)$$
$$\times\{(B_{10}-B_8)[1-.5(\varepsilon_{wc}(2,8)+\varepsilon_{wc}(2,10)]\}+CL(1)\{B_4$$
$$-.5[\varepsilon_{wc}(2,4)(B_4-B_2)+\varepsilon_{wc}(1,2)(B_2-B_1)+\tilde{\varepsilon}_{wc}((0,2),T_1)B_1]\}$$

If the terms $\tilde{\varepsilon}_{wc}((0,2),T_1)B_1$ and $\varepsilon_{wc}(1,2)(B_2-B_1)$ are set to zero in Eq. (3-11) a new parameter can be defined as the net outgoing long-wave radiation and labeled F_2. This parameter was computed to compare with satellite climatological observations over the oceans (Raschke, et al., 1973).

E. APPLICATIONS TO HEAT BALANCE COMPUTATIONS

For computation of the radiative "balance" at the top of the earth-tropospheric system only F_2^* of Eq. (3-11) and the total insolation absorbed below k=2 are required. At the surface, a radiative balance is computed at each gridpoint using the absorbed insolation and the net flux F_{10}^* of Eq. (3-9). Also at the surface a "convective" balance is computed by including the contributions of evaporation and sensible heat transport (see Sec. V). Net flux F_{10}^*, evaporation and sensible heat transport are all considered negative contributions at the surface. The atmospheric radiative balance requires knowledge of the long-wave cooling effects caused by the flux divergences F26 and F610 as defined by:

$$F26 = F_2^* - F_6^* \quad (3\text{-}12a)$$

$$F610 = F_6^* - F_{10}^* \quad (3\text{-}12b)$$

As will be seen in a later section, these parameters act as destabilizing influences in their respective layers when assessed in relationship to other processes in cross sectional display form in Section VI.

F. COMPARISONS WITH PUBLISHED RESULTS

Table II gives a visual comparison of the outgoing longwave radiation, F_2 (as contrasted with F_2*), found by this study as compared to the mean values published by Raschke et al. (1973). Also displayed are this study's global net flux, F_{10}*, computed using Eq. (3-9) as compared to the annual mean deduced from Malkus (1962, Figs. 9,10). The 16 October 1973 results have been interpolated, gridpoint by gridpoint, to 5° latitude increments for each of the four lines (see Fig. 2) and then latitudinally averaged to arrive at the "global" value for each latitude. The units of the values from Malkus (actually due to Budyko (1956)) have been converted from kcal $cm^{-2}yr^{-1}$ to those of cal $cm^{-2}min^{-1}$ used in this study. The global mean values listed at the bottom of each column were derived by cosine weighting the latitudinal values listed in Table II (see also Sec. VII).

It should be noted that the values of F_2 and F_{10}* found by this study for latitudes 20°S, 10°S, and 60°N are averages of only two "sounding" lines while the other latitude values are averaged over all four meridional lines, the difference being due to the number of soundings available near the extremities of the FNWC cross-sections.

The consistently smaller values of net flux, F_{10}*, found by this study might be explained by the fact that Budyko's results are yearly climatological values, whereas the F_{10}* values of this study, involving data from 16 October 1973, occurs near the time of the oceanic maximum of temperature and higher than annual mean cloudiness. This would reduce the net flux F_{10}* computed here. A latitudinal maximum net flux, F_{10}*, was observed around 40°N both for this study and the comparison figures of Malkus. At this location, Figs. 7(b), 9(b), 10(b) show that there was a minimum opaque cloud cover for the time of this study.

The comparison of outgoing long-wave fluxes, F_2 (Table II(b)), appears very consistent when comparing only northern hemispheric latitudes, considering that Raschke's values are based upon the mean for a month rather than that for a single day. Here maximum values of very nearly the same order occur in the subtropics where minimum cloudiness occurs to impede the emission of outgoing terrestrial flux from the earth and lower atmosphere. There is in both this study and in Malkus', a well defined poleward gradient of F_2 by latitudes.

The comparison of the computations of F_{10}* and F_2 made here with climatology (Table IIa,b) cannot confirm or deny the specific cloud-parameterization formulas (Eq. 2-13a,b) used in this study, but they indicate that they have a general reliability.

	(a)		(b)	
LAT	F_{10}* (Malkus)	F_{10}* (This Study)	F_2 (This Study)	F_2 (Raschke et al.)
20°S	.100	.068	.333	.40
10°S	.090	.054	.341	.39
0°	.080	.068	.355	.36
10°N	.090	.079	.378	.34
20°N	.114	.078	.389	.40
30°N	.110	.081	.388	.37
40°N	.120	.107	.376	.34
50°N	.110	.086	.346	.31
60°N	.120	.067	.315	.29
Global Mean	.1018	.0757	.3601	.3615

Table II(a). Comparison of net flux at the surface, F_{10}*, as found by this study for 16 October 1973 and the annual mean F_{10}* derivable from Malkus (1962, Figs. 9,10).

(b). Comparison of net flux to space, F_2, as found by this study and by Raschke et al. (1973), based upon NIMBUS III heat budget studies.

IV. SOLAR RADIATION

A. COMPOSITION OF SOLAR INSOLATION

At the top of the atmosphere (k=0) this study assumed a solar constant of 2.00 ly min^{-1} (Joseph, 1971); furthermore, this constant was assumed subject to a four percent attenuation above the tropopause due to ozone and oxygen. Thus the effective solar constant at level k=2 in this study is 1.92 ly min^{-1}.

To compute the effective solar insolation at the tropopause the following formula was used

$$F(2) = S[\frac{r}{r_m}]^{-2} \text{ Cos } Z \qquad (4\text{-}1)$$

where S = effective solar constant at level k=2

Cos Z = cosine of the zenith angle, a function of the Julian date

r/r_m = ratio of the actual earth-sun distance to the mean earth-sun distance, a function of the Julian date.

The Smithsonian Meteorological Tables (List, 1958) list the ratio r/r_m for 15 October at 0000GMT as 0.997165, this value was utilized for all four data lines. The cosine of the zenith angle was determined by

$$\text{Cos } Z = \text{Sin } \phi \text{ Sin } \delta + \text{Cos } \phi \text{ Cos } \delta \text{ Cos } h \qquad (4\text{-}2)$$

where

ϕ = latitude

δ = solar declination for 15 October = -8° 13.5' (Table 169, List, 1958)

h = hour angle

The value of sine ϕ was calculated using one of two different formulae, depending on the data-line used for the computations, in terms of the FNWC map coordinates (I,J) as in Eq. (4-3a,b), conversely for these lines one may solve for I in terms of sine ϕ as in (4-3c,d):

$$\text{Lines } 1,3,4 \qquad \text{Sin } \phi = \frac{973.752 - 2(32-I)^2}{973.752 + 2(32-I)^2} \qquad (4\text{-}3a)$$

$$\text{Line } 2 \qquad \text{Sin } \phi = \frac{973.752 - (32-I)^2}{973.752 + (32-I)^2} \qquad (4\text{-}3b)$$

$$\text{Lines } 1,3,4 \qquad I = 32 - 22.065 \left[\frac{\text{Cos } \phi}{1 + \text{Sin } \phi}\right] \qquad (4\text{-}3c)$$

$$\text{Line } 2 \qquad I = 32 - 31.205 \left[\frac{\text{Cos } \phi}{1 + \text{Sin } \phi}\right] \qquad (4\text{-}3d)$$

$$I = \begin{cases} 1,\ldots,25 & \text{for Lines } 1,2 \\ 8,\ldots,25 & \text{for Line } 3 \\ 63,\ldots,38 & \text{for Line } 4 \end{cases}$$

Here I is the abscissa distance on the FNWC grid, Fig. 2, and varies by line as described in Sec. II. The soundings for lines 1, 2, and 3 were all taken at 0000GMT with the solar noon existing at the 180^{th} meridian, therefore the hour angles for these three lines were 55°, 10°, and 35°, respectively. For line 4, the soundings were taken 12 hours earlier with solar noon at the Greenwich meridian, giving an hour angle for line 4 of 35°.

The composition of solar insolation was partitioned in this study, in accordance with Joseph (1971), by dividing the insolation, F(2) at level 2, into two parts, one of which was subject to water vapor absorption but not to Rayleigh scattering, F(A), and one which was only subject to Rayleigh scattering, F(S), in a clear moist atmosphere. These partitions may be easily computed as follows:

$$F(A) = 0.349\ F(2) \tag{4-4}$$

$$F(S) = 0.651\ F(2) \tag{4-5}$$

Cloud-reflectivity is inherent in both F(A) and F(S) solar energy portions with the presence of two cloud decks.

To further define the solar insolation partitions, the F(A) energy consists of those wavelengths $\lambda > 0.9$ μm where absorption by water vapor and carbon dioxide bands is the dominant attenuation process for clear air. The F(S) energy is composed of all wavelengths $\lambda \leq 0.9$ μm where water vapor absorption is considered negligible.

B. DISPOSITION OF F(S) INSOLATION

As described by Jenks (1974), there are two reflective-type parameters which must be considered when studying the energy contained in the shorter wavelengths, F(S). The first parameter is the Rayleigh clear-sky albedo, (after Coulson, 1959), which was empirically formulated using the least squares best-fit technique by Joseph (1971) to be

$$\alpha(R) = .085 + .25074 \left[\log_{10} \left(\frac{\pi}{P_0} \text{ Sec } Z\right)\right] \qquad (4\text{-}6)$$

$$P_0 = 1013.25 \text{ mb}$$

Since mean sea level is very nearly 1000 mb, this study assumed that $\pi/P_0 \simeq 1$. The value of Sec. Z is the inverse of Eq. (4-2).

The second reflective parameter considered is the surface albedo, which is a function of the cosine at the zenith angle over ocean surfaces. The surface albedo, as utilized by this study, follows Gates et al. (1971).

$$\alpha(G) = \max \{.06, .06 + .54 (.7 - \text{Cos } Z)\} \qquad (4\text{-}7)$$

As described in Sec. III, four distinct cloud cases are possible with a two-layer cloud model. The disposition of F(S) under each of these cases will be discussed in the remainder of this subsection.

1. Clear Sky Case

With clear sky the F(S) insolation is modified only by Rayleigh sky reflectivity, $\alpha(R)$, and surface reflectivity, $\alpha(G)$, as given by Eqs. (4-6) and (4-7). Jenks (1974)points out that with multiple reflections possible between the earth and atmosphere, the clear sky insolation absorbed at the earth's surface (k=10) after scattering is given by

$$IS10(0,0) = F(S)[1-\alpha(R)][1-\alpha(G)]/[1-\alpha(R)\alpha(G)] \qquad (4\text{-}8)$$

where the notation (0,0) denotes CL(1) = CL(2) = 0.0 as discussed in section III.

2. Cloudy Sky Cases

With the presence of cloud layers, an additional insolation modifier must be considered, cloud reflectivity. In this study the values suggested by C.D. Rodgers (1967) were adopted, namely, R(1) = 0.54 for the higher clouds (between k=4 and k=6) and R(2) = 0.66 for the lower clouds (between k=8 and k=9).

Consider first the case (1,0) where the fraction of the grid area has overcast clouds only at the high level, that is where CL(1) = 1.0, CL(2) = 0.0, and R(2) = 0.0 so that the earth-absorbed F(S) insolation is

$$IS10(1,0) = F(S)(1-R(1))(1-\alpha(G))/(1-R(1)\alpha(G)) \qquad (4\text{-}9)$$

The F(S) insolation absorbed by the surface above which there is present only a lower cloud overcast, [denoted by (0,1)] where CL(1) = 0.0, CL(2) = 1.0, and R(1) = 0.0 is given by

$$IS10(0,1) = F(S)(1-R(2))(1-\alpha(G))/(1-R(2)\alpha(G)) \qquad (4\text{-}10)$$

If overcast clouds are present in both layers, then the conditions CL(1) = CL(2) = 1.0 [or in abbreviated symbolism, case (1,1)] applied, and reflectance also exists between the cloud layers as well as between clouds and space. Thus the absorbed F(S) insolation at the earth's surface as formulated after Arakawa (1972) is given by

$$IS10(1,1) = F(S)[(1-R(1))(1-R(2))(1-\alpha(G))]/[1-((R(1)R(2) + R(2)\alpha(G)+R(1)\alpha(G))+2(R(1)R(2)\alpha(G))] \qquad (4\text{-}11)$$

a formula which resembles very closely a combination of Eqs. (4-9) and (4-10).

Thus far in this subsection the sky was considered either overcast or clear at each level without regard for the actual cloud conditions CL(1) and CL(2).

3. Composite F(S) Insolation

If the areal coverage weights, as defined by Eq. (3-4), are applied to the appropriate right sides of Eqs. (4-8), (4-9), (4-10), and (4-11), then the composite surface-absorbed insolation, IS10, results

$$IS10 = IS10(0,0)W(0,0)+IS10(1,0)W(1,0) + IS10(0,1)W(0,1)+IS10(1,1)W(1,1) \quad (4\text{-}12)$$

It is apparent that F(S) insolation reflected to space may be found by subtracting IS10 from F(S).

C. DISPOSITION OF F(A) INSOLATION

This subsection deals with that portion of the solar insolation which is absorbed by atmospheric water vapor and carbon dioxide, namely the longer wavelengths. The discussion will again be divided into the four different cloud-layer cases.

1. The Clear Sky Case

Formulation enabling the determination of absorption values for particular layers of interest was provided by use of the Manabe-Möller absorptivity function which may be generalized as follows

$$\underline{a}(2,2k) = .271[U(2,2k)\ \mathrm{Sec}\ Z]^{.303} \quad (4\text{-}13)$$

Here absorptivity $\underline{a}$ is applied over the pressure-scaled water vapor mass between levels 2 and 2k (Fig. 1) along the slant path of the zenith angle Z. Recalling that the water vapor mass above level 2 was assumed negligible, the absorbed solar insolation, for example, in the layer (2,6) is written as

$$A(2,6) = 0.271\ F(A)[U(2,6)\ \text{Sec}\ Z]^{\cdot 303} \qquad (4\text{-}14)$$

and the absorbed solar insolation in the layer (6,10) is given by

$$A(6,10) = A(2,10) - A(2,6) \qquad (4\text{-}15)$$

For a schematic depiction of the F(A) insolation disposition in the clear sky case [see Fig. 3 in Jenks (1974)].

To obtain that portion of F(A) insolation which is absorbed at the earth's surface, the atmospheric transmissivity (1-$\underline{a}$(2,10)) and the surface transmissivity after reflectance are combined (by the product-law of transmissivities) to give IA10 as follows:

$$IA10(0,0) = F(A)\{1-.271[U(2,10)\ \text{Sec}\ Z]^{\cdot 303}\}(1-\alpha(G)) \qquad (4\text{-}16)$$

Here $\alpha(G)$ is defined by Eq. (4-7)

In the remainder of this subsection, which discusses the cloudy layer cases, representative cloud reflectivities and cloud absorptivities were adopted, after C.D. Rodgers (1967), for the two possible cloud layers. The cloud reflectivities were RA(1) = .46 and RA(2) = .50 while the cloud absorptivities were A(1) = .20 and A(2) = .30. Note that the reflectivities for the F(A) wavelengths differ from

those adopted for the F(S) wavelengths. The procedure of considering the cloud conditions to be overcast whenever they appear and then applying the appropriate weighting factors in the composite summation will again be followed as in Sec. IV.B.

To simplify the discussion for the cloud-covered cases, the (1,1) case will be presented first as it contains representative type equations for the remaining two cases, (1,0) and (0,1).

2. Overcast in Both High and Low Cloud Layers

The following set of formulas detail the disposition of incoming solar insolation (F(A)) from level k=2 to the earth's surface to permit determination of the amount of insolation absorbed by the atmospheric layers and by the earth's surface. The dashed separation lines are introduced to subdivide the absorption and reflection physics of the model into subsections which permit the analysis to proceed more or less within successive 200 mb layers (see also Fig. 3).

$$
\begin{aligned}
F4\downarrow &= F(A)(1-.271[U(2,4)\ \mathrm{Sec}\ Z]^{\cdot 303}) \\
F4\uparrow &= F4\downarrow(RA(1)) \\
A24\downarrow &= F(A).271[U(2,4)\ \mathrm{Sec}\ Z]^{\cdot 303} \\
A24\uparrow &= F4\uparrow.271[U(2,4)\ \mathrm{Sec}\ Z]^{\cdot 303}
\end{aligned}
\qquad (4\text{-}17a)
$$

- -

$$
\begin{aligned}
F6\downarrow &= F4\downarrow(1-RA(1)-A(1)) \\
A46 &= F4\downarrow(A(1)) \\
A26 &= A24\downarrow + A24\uparrow + A46
\end{aligned}
\qquad (4\text{-}17b)
$$

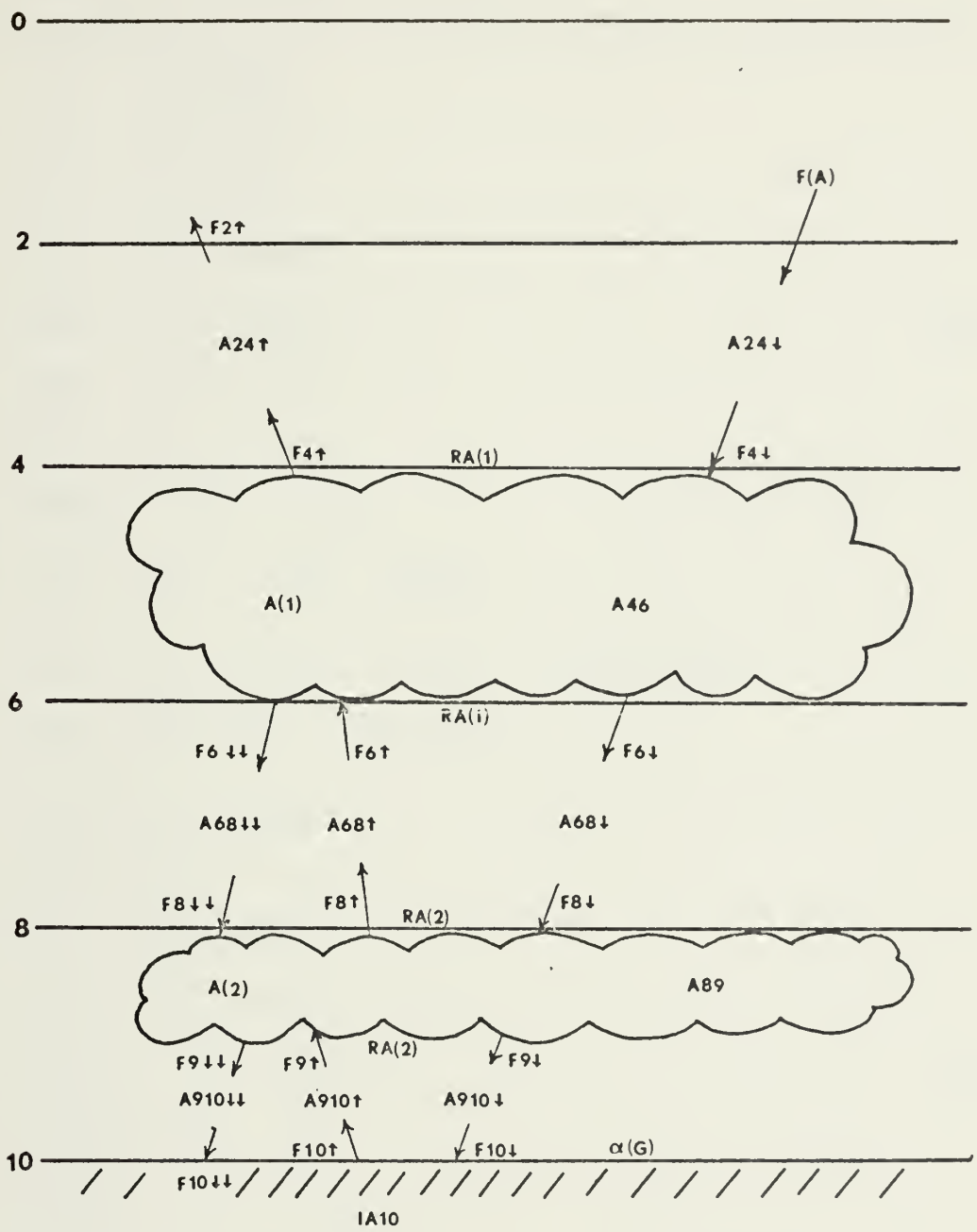

Figure 3. Schematic representation of F(A) insolation disposition in the case of two overcast layers.

$$TD68 = 1-.271[U(6,8)5/3]^{.303}$$

$$TD910 = 1-.271[U(9,10)5/3]^{.303} \qquad (4\text{-}18)$$

$$F8\downarrow = F6\downarrow(TD68)$$

$$F8\uparrow = F8\downarrow(RA(2))$$

$$F6\uparrow = F8\uparrow(TD68)$$

$$F6\downarrow\downarrow = F6\uparrow(RA(1))$$

$$F8\downarrow\downarrow = F6\downarrow\downarrow(TD68) \qquad (4\text{-}19a)$$

$$A68\downarrow = F6\downarrow - F8\downarrow$$

$$A68\uparrow = F8\uparrow - F6\uparrow$$

$$A68\downarrow\downarrow = F6\downarrow\downarrow - F8\downarrow\downarrow$$

$$A68 = A68\downarrow + A68\uparrow + A68\downarrow\downarrow$$

- -

$$F9\downarrow = F8\downarrow(1-RA(2) - A(2)) + F8\downarrow\downarrow(1-A(2)) \qquad (4\text{-}19b)$$

$$A89 = F8\downarrow(A(2)) + F8\downarrow\downarrow(A(2))$$

- -

$$F10\downarrow = F9\downarrow(TD910)$$

$$F10\uparrow = F10\downarrow(\alpha(G))$$

$$F9\uparrow = F10\uparrow(TD910)$$

$$F9\downarrow\downarrow = F9\uparrow(RA(2))$$

$$F10\downarrow\downarrow = F9\downarrow\downarrow(TD910) \qquad (4\text{-}19c)$$

$$A910\downarrow = F9\downarrow - F10\downarrow$$

$$A910\uparrow = F10\uparrow - F9\uparrow$$

$$A910\downarrow\downarrow = F9\downarrow\downarrow - F10\downarrow\downarrow$$

$$A910 = A910\downarrow + A910\uparrow + A910\downarrow\downarrow$$

$$A810 = A89 + A910$$

- -

In the preceding equations the symbol "A" followed by a set of digits refers to the F(A) insolation absorbed in the indicated layer, for example, A26 indicates the absorption in the layer k=2 to k=6. The symbol "F" followed by a k value indicates the amount of insolation passing through the particular k level. The vertical arrow modifiers indicate the direction of insolation passage, i.e., ↓ downward insolation, ↑ upward reflected insolation, and ↓↓ downward reflected insolation. Terms involving the symbols "TD" as expressed by the functions of Eq. (4-18), indicate the Manabe-Möller transmissivities for insolation beneath a cloud layer. In the latter situation, the term Sec Z in Eq. (4-13) is effectively replaced by the mean slant-path $\overline{\text{Sec Z}} \simeq 5/3$ (Katayama, 1966).

Note that the effect of multiple reflections between clouds or between the earth's surface and the lower cloud has been incorporated to the extent of two reflections, with the lowermost reflecting surface absorbing the remaining impinging insolation. Computations indicated that the insolation remaining after two reflections was too small to warrant further reflections. Also insolation reflected upward from a lower interface (cloud or ground) to the base of an upper cloud deck has not been subjected to cloud absorption. This tends to reduce very slightly the secondary cloud-absorption.

Note finally that between any two reflecting surfaces there are three contributions to absorption of solar insolation within the layer. These contributions are denoted by

the arrow-identifiers which indicate the segment of path being traversed.

From Eqs. (4-19c) the impinging F(A) insolation at the earth's surface can be expressed

$$TRANA(1,1) = F10\downarrow + F10\downarrow\downarrow \qquad (4\text{-}20)$$

The F(A) insolation which is actually absorbed by the earth's surface (see Fig. 3) may be written as

$$IA10(1,1) = F10\downarrow(1-\alpha(G)) + F10\downarrow\downarrow \qquad (4\text{-}21)$$

3. Disposition of F(A) Insolation with an Upper Overcast

With a cloud layer present only in the upper layer the equations depicting the disposition of incoming insolation becomes a simplified subset of the previous case:

$$A24\downarrow = F(A).271[U(2,4)\ \text{Sec}\ Z]^{.303}$$

$$A24\uparrow = F(A)\{1-.271[U(2,4)\ \text{Sec}\ Z]^{.303}\}RA(1) \times\{.271[U(2,4)\ \text{Sec}\ Z]^{.303}\} \qquad (4\text{-}22a)$$

$$A24 = A24\downarrow + A24\uparrow$$

- -

$$F6\downarrow = F(A)\{1-.271[U(2,4)\ \text{Sec}\ Z]^{.303}\}[1-RA(1)-A(1)]$$

$$A46 = F(A)\{1-.271[U(2,4)\ \text{Sec}\ Z]^{.303}\}A(1) \qquad (4\text{-}22b)$$

$$A26 = A24 + A46$$

- -

$$F10\downarrow = F6\downarrow(TD610)$$

$$F10\uparrow = F10\downarrow(\alpha(G))$$

$$F6\uparrow = F10\uparrow(TD610)$$

$$F6\downarrow\downarrow = F6\uparrow(RA(1))$$

$$F10\downarrow\downarrow = F6\downarrow\downarrow(TD610) \qquad (4\text{-}22c)$$

$$A610\downarrow = F6\downarrow - F10\downarrow$$

$$A610\uparrow = F10\uparrow - F6\uparrow$$

$$A610\downarrow\downarrow = F6\downarrow\downarrow - F10\downarrow\downarrow$$

$$A610 = A610\uparrow + A610\downarrow + A610\downarrow\downarrow$$

The variables used above are defined in a similar manner to those in the (1,1) case. The impinging insolation at the earth's surface may be formulated as follows

$$TRANA(1,0) = F10\downarrow + F10\downarrow\downarrow \qquad (4\text{-}23)$$

while the F(A) insolation absorbed by the earth in this case (Fig. 4) is given by

$$IA10(1,0) = F10\downarrow(1-\alpha(G)) + F10\downarrow\downarrow \qquad (4\text{-}24)$$

4. Disposition of F(A) Insolation with a Low Overcast

With an overcast lower cloud layer the disposition formulas are as follows:

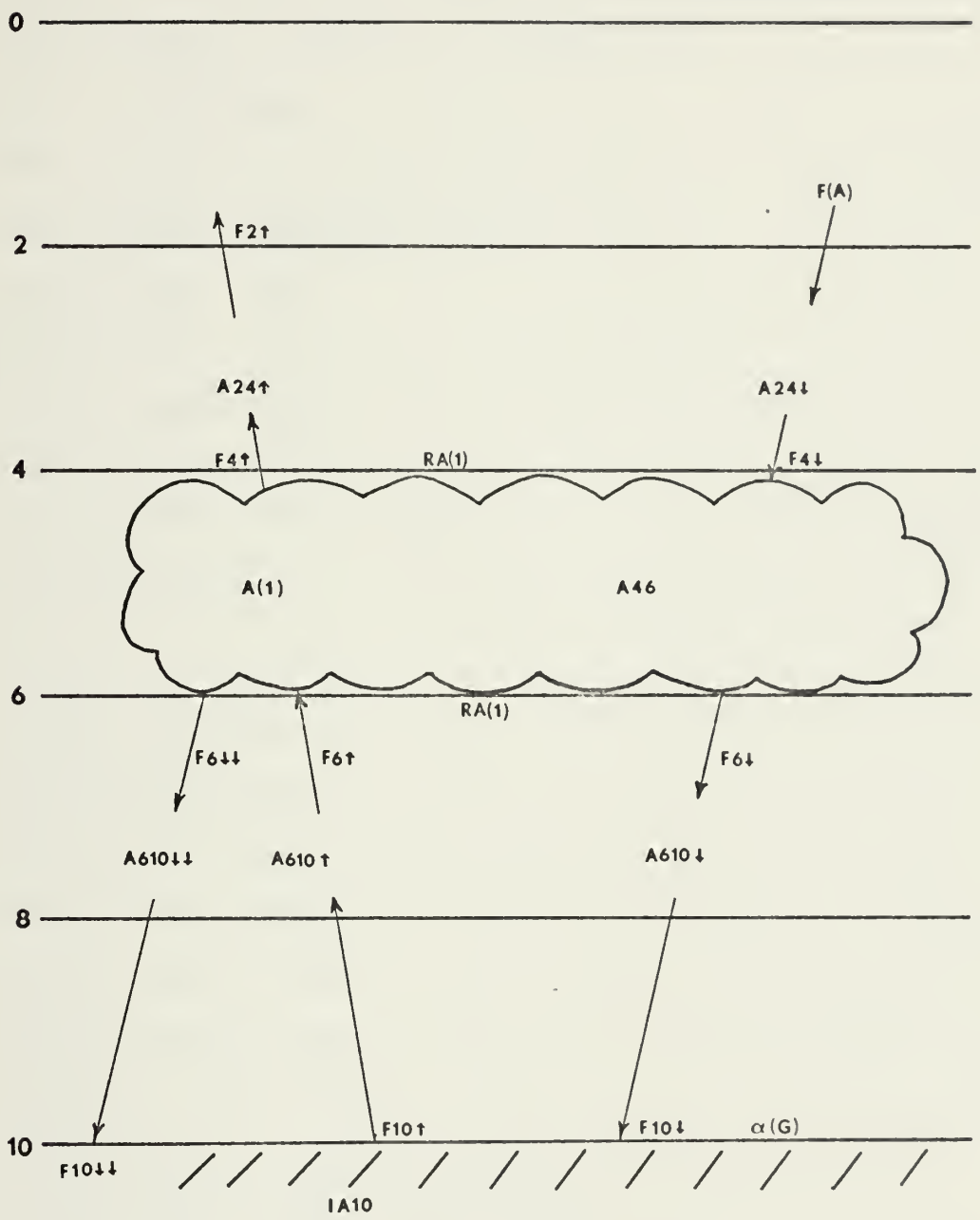

Figure 4. Schematic representation at F(A) insolation disposition with an upper overcast layer only.

$$A26\downarrow = F(A).271[U(2,6)\ \text{Sec}\ Z]\cdot^{303}$$

$$A68\downarrow = F(A).271\{[U(2,8)\ \text{Sec}\ Z]\cdot^{303} - [U(2,6)\ \text{Sec}\ Z]\cdot^{303}\}$$

$$F8\downarrow = F(A)\{1-.271[U(2,8)\ \text{Sec}\ Z]\cdot^{303}\}$$

$$F8\uparrow = F8\downarrow[RA(2)]$$

$$F6\uparrow = F8\uparrow\{1-.271[U(6,8)\ \text{Sec}\ Z]\cdot^{303}\} \qquad (4\text{-}25a)$$

$$F2\uparrow = F8\uparrow\{1-.271[U(2,8)\ \text{Sec}\ Z]\cdot^{303}\}$$

$$A68\uparrow = F8\uparrow - F6\uparrow$$

$$A26\uparrow = F6\uparrow - F2\uparrow$$

$$A26 = A26\downarrow + A26\uparrow$$

- -

$$F9\downarrow = F8\downarrow[1-RA(2) - A(2)]$$

$$A89 = F8\downarrow[A(2)] \qquad (4\text{-}25b)$$

- -

$$F10\downarrow = F9\downarrow(TD910)$$

$$F10\uparrow = F10\downarrow(\alpha(G))$$

$$F9\uparrow = F10\uparrow(TD910)$$

$$F9\downarrow\downarrow = F9\uparrow(RA(2))$$

$$F10\downarrow\downarrow = F9\downarrow\downarrow(TD910) \qquad (4\text{-}25c)$$

$$A910\downarrow = F9\downarrow - F10\downarrow$$

$$A910\uparrow = F10\uparrow - F9\uparrow$$

$$A910\downarrow\downarrow = F9\downarrow\downarrow - F10\downarrow\downarrow$$

$$A910 = A910\downarrow + A910\uparrow + A910\downarrow\downarrow$$

$$A610 = A68\downarrow + A68\uparrow + A89 + A910$$

Again the variables are defined as stated before in the (1,1) case. Likewise the incident flux is defined at the earth's surface as

$$TRANA(0,1) = F10\downarrow + F10\downarrow\downarrow \qquad (4\text{-}26)$$

while that portion which is absorbed by the earth, (Fig. 5) is

$$IA10(0,1) = F10\downarrow(1-\alpha(G)) + F10\downarrow\downarrow \quad (4\text{-}27)$$

5. Weighted F(A) Layer-Absorptions and Surface-Absorption Insolation

As described in Section IV.B.3 on the composite F(S) insolation, the values of the absorbed F(A) insolation in the layers and of the earth's surface which were calculated for the four cloud cases (0,0), (1,0), (0,1), and (1,1) must be appropriately weighted by the values from Eq. (3-4) to obtain the composite F(A) layer- and surface-absorbed insolation.

$$A26 = A26_{(0,0)}W(0,0)+A26_{(1,0)}W(1,0)+A26_{(0,1)}W(0,1) + A26_{(1,1)}W(1,1) \quad (4\text{-}28)$$

$$A610 = A610_{(0,0)}W(0,0)+A610_{(1,0)}W(1,0)+A610_{(0,1)}W(0,1) + A610_{(1,1)}W(1,1) \quad (4\text{-}29)$$

$$IA10 = IA10(0,0)W(0,0)+IA10(1,0)W(1,0)+IA10(0,1)W(0,1) + IA10(1,1)W(1,1) \quad (4\text{-}30)$$

6. Absorptivity (ABA) by Layers

It was convenient to work with the absorptivity as well as the actual insolation energies absorbed by each layer and at the surface. To obtain the absorptivity, the total incoming insolation at k=0 must be known. This value called FADJ is formulated as follows

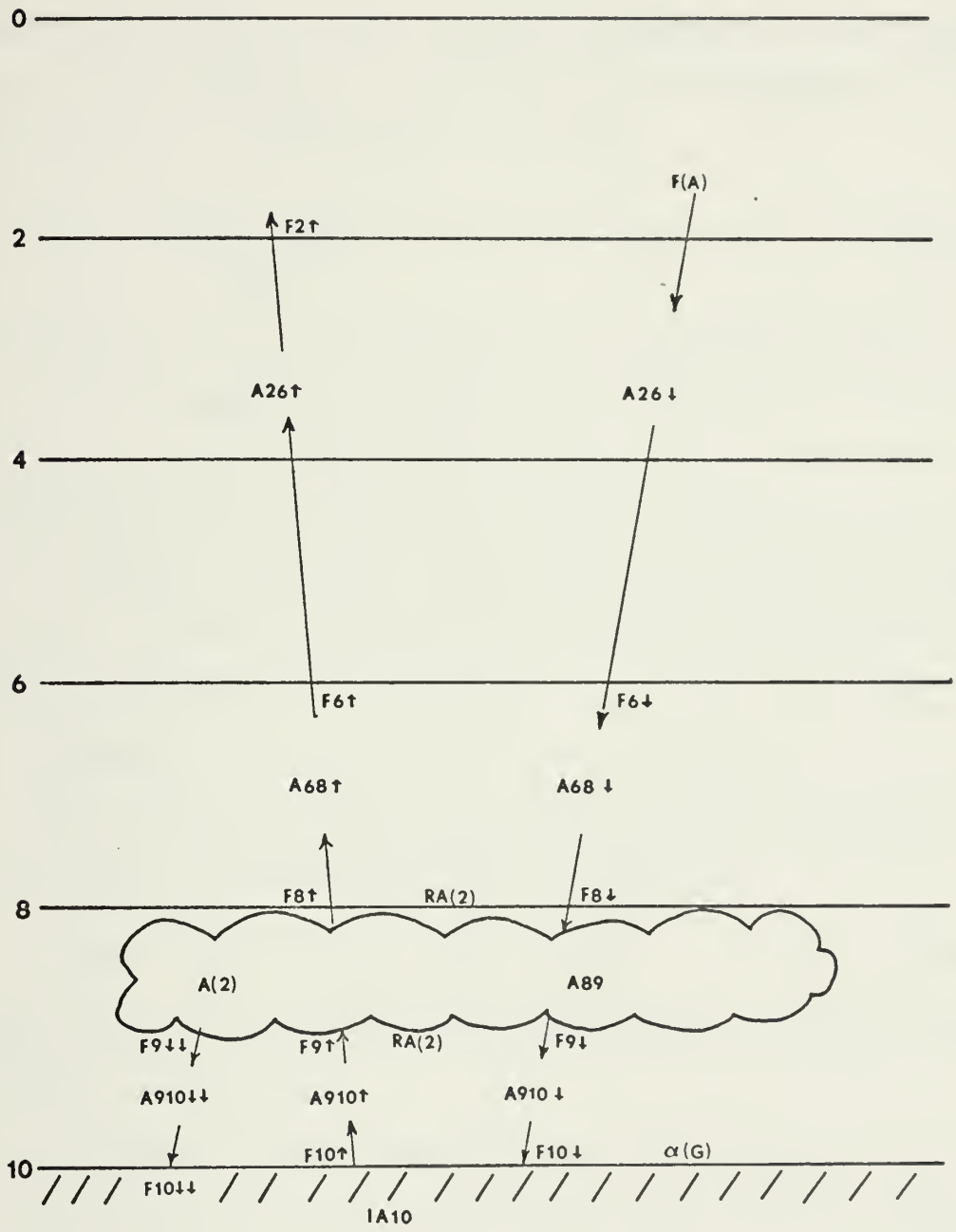

Figure 5. Schematic representation of F(A) insolation disposition with a lower overcast layer only.

$$FADJ = 2.00\ (r/r_m)^{-2}\ \text{Cos}\ Z \qquad (4\text{-}31)$$

By taking the ratio of the insolation absorbed in the troposphere to that incident at the top of the atmosphere, the full tropospheric absorptivity is formed

$$ABA = \frac{A26 + A610}{FADJ} \qquad (4\text{-}32)$$

Similar formulas may be expressed for the partial absorptivities for the layers (2,6) and (6,10).

D. REFLECTION OF F(A) AND F(S) ENERGY

To determine the albedo and fractional absorptivity of the earth's surface, both the F(A) and F(S) fractions of solar insolation must be considered.

1. Albedo

The amount of F(A) insolation which is reflected back to space is determined by the following

$$REFA = F(A) - A26 - A610 - IA10 \qquad (4\text{-}33)$$

here A26, A610, and IA10 are defined by Eqs. (4-28), (4-29), and (4-30), respectively.

Because the F(S) wavelengths do not undergo atmospheric absorption, the reflected F(S) insolation was easier to calculate

$$REFS = F(S) - IS10 \qquad (4\text{-}34)$$

IS10 was defined by Eq. (4-12). By combining Eqs. (4-33) and (4-34) the total reflected insolation to space is defined by

$$REF = REFA + REFS \tag{4-35}$$

The resulting REF values were calculated at each gridpoint and are meridionally displayed by latitudinal interpolation in Figs. 7(a),...,10(b).

By taking the ratio of the total reflected energy to the total incoming energy the earth-atmospheric system albedo is defined

$$ALB = REF/FADJ \tag{4-36}$$

where FADJ is defined by Eq. (4-31).

2. Composite Absorptivity (ABG) by the Earth's Surface

The fractional absorptivity of the earth's surface was determined by the ratio of the total insolation absorbed by the earth to the total incoming insolation. The total insolation absorbed by the surface is determined by the properly weighted sums of IA10 and IS10, defined by Eqs. (4-30) and (4-12), respectively.

$$ABG = (IA10 + IS10)/FADJ \tag{4-37}$$

The result of Eq. (4-37) gives the weighted absorptivity of earth. It is also of interest to determine the total insolation incident at the earth's surface just before absorption by earth. The result is given by the properly weighted sum of terms of the form

$$TRAN = TRANA + [IS10/(1-\alpha(G))] \tag{4-38}$$

It should be noted that each of the four terms of form IS10 (Eq. 4-12) had a factor $(1-\alpha(G))$ in the numerator so that the transmitted F(S) insolation incident at earth before absorption need only be divided by $(1-\alpha(G))$. The parameter TRAN is a simulation of the insolational energy incident at a pyrheliometer. Note finally that the ratio

$$\text{ATRAN} \equiv \text{TRAN/FADJ} \tag{4-39}$$

represents the transmissivity of the troposphere.

3. Computational Check

Recalling the assumption of a four percent attenuation of the incoming solar insolation in the stratosphere, the summation of the fractional absorptivities ALB, ABA, and ABG should equal 0.96. This value provides a good computational check for this model at each gridpoint and was in fact satisfied over the entire grid.

E. STATISTICAL TESTS

To further verify the foregoing calculations, statistical computations were performed on several key parameters utilizing linear regression techniques from the BMD set of statistical computer programs (Dixon, 1973).

1. Clear Sky Case Regressions

Three linear regressions were computed for the clear sky case, the first of which was the clear sky albedo, ALB(0,0,Z). The best-fit equation, using the secant of the zenith angle, Sec Z, as the predictor, was computed to be

$$\text{ALB}(0,0,Z) = 0.00650 + 0.09052 \text{ Sec } Z \tag{4-40}$$

with a regression coefficient R = .964. This highly significant correlation coefficient confirms the model results which indicate that Sec Z is a good predictor of clear-sky albedo. In this connection, it should be recalled that $\alpha(G)$ and $\alpha(R)$ were modeled to be functionally related to Sec Z. The mean global clear-sky albedo was

$$\overline{ALB(0,0)} = 0.164$$

which corresponds to the mean secant of the zenith angle, $\overline{Sec\ Z} = 1.743$, for this study. The statistics show that the largest contributions to error in the fit by Eq. (4-40) occurred at largest zenith angles, which occur at high latitudes.

The two other clear-sky linear regressions performed were ABA(0,0,M) and ATRAN(0,0,M), where the predictor, M, was the water-vapor mass path length given by

$$M = (U\ Sec\ Z)^{\frac{1}{2}}[\log_{10}(U\ Sec\ Z)^{\frac{1}{2}}] \qquad (4\text{-}41)$$

This parameterization of the water-vapor mass is formulated after Hanson (1967, 1971), who used a similar absorber-mass predictor in his empirical equations for ABA with both clear and partly cloudy skies. The resulting clear-sky regression equations in this study for ABA and ATRAN were

$$ABA(0,0,M) = 0.10320 + 0.05535M \qquad (4\text{-}42)$$

with R = .9925 and

$$ATRAN(0,0,M) = 0.77494 - 0.04823M \qquad (4\text{-}43)$$

with R = .7142. The sample means of the statistics which entered into (4-42) and (4-43) are

$$\overline{ABA(0,0,M)} = 0.146$$

$$\overline{ATRAN(0,0,M)} = 0.738$$

$$\overline{M} = 0.776 \text{ (gm cm}^{-2})^{\frac{1}{2}}$$

based on the original 93 cases.

2. Cloudy-Sky Case Regressions

In addition to the clear-sky fractional amounts of ALB, ABA, and ATRAN, linear regressions were formulated for the composite cloudy-sky case, i.e. ALB[CL(1),CL(2)], ABA[CL(1),CL(2)], and ATRAN[CL(1),CL(2)], respectively. The regression relationships between the clear- and cloudy-sky cases were determined for the same zenith angle at gridpoint (I,J) using the total opaque cloud cover (CL) as the predictor. The total opaque cloud cover approximates the effective cloud cover existing in a two-layer cloud model and is expressed as

$$CL = CL(1) + CL(2) - CL(1)CL(2) \qquad (4\text{-}44)$$

The relationship between the cloudy-sky albedo and the corresponding clear-sky calculation was obtained by least squares with the following results

$$ALB[CL(1),CL(2)] = ALB(0,0)[1+2.09929CL+0.84608CL^2] \qquad (4\text{-}45)$$

and R = .9292. The means of the parameters used in Eq. (4-45) are

$\overline{ALB[CL(1),CL(2)]} = 0.406$

$\overline{ALB(0,0)} = 0.164$

$\overline{CL} = 0.662$

The dependence of Eq. (4-45) upon CL is indicated by the high correlation coefficient (R=.9292). The global mean albedo for this study of 0.406 is somewhat higher than that reported in recent literature (ALB=.300) by Raschke et al. (1973). However, Raschke's figure is an annual mean which includes the somewhat smaller cloud amounts over land.

The tropospheric absorptivity of air in the composite cloudy case was developed analogously to (4-45) by least squares and gave the form

$$ABA[CL(1),CL(2)] = ABA(0,0)[1+0.22305CL+0.17261CL^2] \quad (4\text{-}46)$$

with R = .927 and mean statistics for the above parameters

$\overline{ABA[CL(1),CL(2)]} = 0.180$

$\overline{ABA(0,0)} = 0.146$

$\overline{CL} = 0.662$

The direct relationship between solar absorptivity and cloud cover is in general agreement with the results of Plante (1972) who found increased absorptivity with increasing CL. This relationship could be the reason for the recent reduced estimates of global albedo [Raschke et al. (1973), Vonder Haar and Suomi (1971)]. The significant value of R indicates the degree of sensitivity between cloud amounts and atmospheric absorptivity.

The final statistical regression equation formulated deals with the cloud-sky transmissivity of the troposphere relative to the clear-sky calculation. Again the total opaque cloud cover has been used as the independent variable

$$ATRAN[CL(1),CL(2)] = ATRAN(0,0)[1-0.51477CL-0.14646CL^2] \quad (4-47)$$

Here the correlation coefficient R = .997 and the mean statistics over the 93 sample soundings are

$$\overline{ATRAN[CL(1),CL(2)]} = 0.543$$

$$\overline{ATRAN(0,0)} = 0.738$$

$$\overline{CL} = 0.662$$

Note the high degree of significance, (R = .997) of Eq. (4-47), which formulation agrees with empirical results of Quinn (1971) and numerous other workers cited by Quinn in his 1971 paper.

In general, the solar-model statistical relationships developed in this study show consistency with empirically reported observations, which have already been noted, when consideration is taken for seasonal effects and the latitudinal limits of this study.

V. SENSIBLE AND LATENT HEAT TRANSPORT AT THE SEA-AIR INTERFACE

A. GENERAL CONSIDERATIONS

For a complete discussion of the heat balances of the earth and atmosphere for 16 October 1973, the vertical transports of sensible and of latent heats across the sea-air interface must be considered. For this purpose, the turbulent flux models for the planetary boundary layer, as used in the FNWC primitive equation model as described by Kesel and Winninghoff (1972) and Kaitala (1974) , was adapted here virtually without change.

B. EVAPORATION

The determination of the surface latent heat flux, E, over the ocean is based upon its large scale parameterization, principally after Langlois and Kwok (1969)

$$E = L\rho_{10}\frac{K^*}{1+a^*\left(\frac{\theta_9-\theta_s}{Z_9-Z_{10}}\right)}\left[\frac{q_x-q_9}{Z_9-Z_{10}}\right] \qquad (5\text{-}1)$$

Here L is the latent heat of vaporization given by

$$L = 596.73 - .601\ T_{10} \quad (cal/gm)$$

The other parameters in (5-1) are formulated as follows:

$$\rho_{10} = P_{10}/R_d T_{10}$$

$$\theta_9 = T_9\left(\frac{1000}{900}\right)^{2/7}$$

$$\theta_s = T_{10}$$

$$Z_9 - Z_{10} = \frac{R_d}{g} \overline{T}^{9-10} \ln \frac{1000}{900}$$

$$q_x - q_9 = .62197 \frac{e_x}{1000} - q(900)$$

Note that at level k=10, the assumption $P_{10} \simeq 1000$ mb is considered valid and e_x is the vapor pressure at the top of the constant flux layer. Also q(900) is the mixing ratio at k=9 as defined by Eq. (2-4). In Eq. (5-1) K* and a* are turbulent transfer coefficients having values 2×10^5 cm^2 sec^{-1} and 5×10^4 cm/°K, respectively, according to Kaitala (1974). However, values of the eddy coefficient, K*, of 2×10^5 and 1×10^5 were both tested in this study and it was decided primarily to use only the latter value. Furthermore, it is felt by this author that upon further testing, with a broader data base, it may be feasible to tune K* between the two values tested so as to make it dependent either upon latitude or season, or other pertinent variables.

C. SENSIBLE HEAT TRANSPORT

Sensible heating is computed as a function of the temperature difference between the surface, T_{10}, and the air near the surface, T_x, which is at the top of the constant flux layer. Since wind values were not carried in this study, the technique used by Mintz and Arakawa, as described by Kaitala (1974) and by Kesel and Winninghoff (1972), was first attempted for sensible heating

$$H_\Gamma = \rho_{10} C_p \left(\frac{K^*}{1+a^*\left(\frac{\theta_9-\theta_S}{Z_9-Z_{10}}\right)}\right)\left\{\gamma_c - \frac{\theta_9-\theta_x}{Z_9-Z_{10}}\right\} \qquad (5\text{-}2)$$

Here C_p = .239 cal/(gm°K), and, since the constant flux layer was assumed to be quite thin, $\theta_x = T_x$. γ_c is a critical lapse rate (3×10^{-5} °K/cm), and the remainder of the terms are defined as in the discussion following Eq. (5-1). The micrometeorological equivalent of Eq. (5-2) is given by Kaitala (1974) as

$$H_\Gamma = \rho_{10} C_p C_D V_S (T_g - T_x) \qquad (5\text{-}3)$$

It can be seen from Eqs. (5-2), (5-3) that the temperature lapse, $T_g - T_x$, for the thin layer between the surface and the top of the constant flux layer becomes very critical in determining the amount of sensible heating (cooling) for each sounding location.

In Eq. (5-2), the expression within the brace determined the sign of the sensible heat flux in the vertical. In approximately one out of three cases, the braced expression gave rise to negative values of H_Γ, whereas the corresponding latent heat flux, E, of Eq. (5-1) was systematically positive. Based on Fig.15 in Malkus (1962), which shows $H_\Gamma > 0$, there seems to be no valid basis for having an erratically downward distribution of sensible heat over the open oceans. Consequently, this study assumed that E was properly assessed by Eq. (5-1), and that a reasonable set of values of H_Γ could be obtained by means of

$$H_\Gamma = rE \tag{5-4}$$

Here the Bowen ratio r was determined from a set of best estimates as a function of latitude.

Using 20 values of r and their functionally related latitudes, taken from published results of Sellers (1965), Budyko (1956), and Jacobs (1951), a linear regression was best-fitted to $|\text{Sin } \phi|$ to give

$$r = 0.10910 - .41996\ |\text{Sin } \phi| + .89645\ |\text{Sin } \phi|^2 \tag{5-5}$$

with a correlation coefficient of R = .982. Thus, using Eqs. (5-4) and (5-5), the sensible heat transport was obtained at each gridpoint, while always maintaining proper sign sense with E which was virtually always positive.

D. COMBINED TURBULENT HEAT FLUX ACROSS THE SEA-AIR INTERFACE

To get a better feel for the effect that sensible heating has at the surface, the summed terms E and H_Γ were utilized as heat-loss quantities in the total budget at the surface, therefore in terms of large scale "convective" disposition

$$E + H_\Gamma = E(1+r) \tag{5-6}$$

where r ranges in magnitude from approximately .05 to .5 with increasing latitude.

VI. MERIDIONAL CROSS-SECTIONAL DEPICTION OF THE HEATING MODEL COMPUTATIONS

A. GENERAL DESIGN OF HEAT-MODEL OUTPUT

In this section, the computational subroutines already developed (Secs. III, IV, and V) are combined to perform a single time-step of the heating program developed for adaptation to the FNWC prediction model. The results represent computations of the relevant heating functions at each gridpoint of the four meridians (Fig. 2).

For the three Pacific cross-sections, the FNWC gridpoint-processed analyses for 0000GMT, 16 October 1973, have been used, whereas for the 35°W (Atlantic) meridian, the FNWC analyses from 1200GMT, 15 October 1973, were utilized. For simplicity the heating model computations will be referred to as those pertaining to 16 October 1973.

Fig. 6 depicts the key to the computations made at (I,J) gridpoint soundings, shown in the form of Table I(b), and in effect represents the flow diagram of computations proceeding from top-to-bottom at each gridpoint. Figs. 7, 8, 9, and 10 show that the gridpoints considered are at 5° latitude increments, but this has been done merely for simplification of the interpretations and for comparisons with climatological data. In order to deduce a heating parameter, Q(I), at a non-integral grid-value I corresponding to latitude ϕ (in whole multiples of 5°), a Lagrangian cubic interpolation scheme was utilized of the form

$$Q(I) = \frac{Q_1(I-2)(I-3)(I-4)}{(1-2)(1-3)(1-4)} + \frac{Q_2(I-1)(I-3)(I-4)}{(2-1)(2-3)(2-4)} + \frac{Q_3(I-1)(I-2)(I-4)}{(3-1)(3-2)(3-4)} + \frac{Q_4(I-1)(I-2)(I-3)}{(4-1)(4-2)(4-3)} \quad (6\text{-}1)$$

Here I is determined by an equation of the form (4-3c), the points 1,2,3, and 4 are any four successive integral values of I with I lying in general between points 2 and 3, although the subroutine also works well if I is non-centered in the I-array.

B. CROSS-SECTIONAL DATA AT LEVEL k=2

The terms explained here are those occurring at the level k=2. The discussion of all insolational parameters discussed previously in section IV pertained to the specific time of day corresponding to the hour angle h at the instantaneous times under consideration. Thus the incident insolation was given by Eq. (4-1), i.e.

$$F(2) = S\,(\frac{r}{r_m})^{-2}\,\text{Cos}\,Z$$

with Cos Z given by Eq. (4-2). For the specific map times the local solar times gave h=35°, 10°, 55°, and 35° for cross-sections 1,2,3, and 4 depicted in Figs. 7, 8, 9, and 10 respectively.

For each specific zenith angle Z corresponding to latitude $\phi(I,J,t)$ the absorbed insolations A(2,6,t) and A(6,10,t) of Eqs. (4-28) and (4-29) have been determined for the given time t of 16 October 1973 for which the specific hour angles were applicable. The instantaneous parameter REF(t) of Eq. (4-35) was determined by the equation

$$REF(t) = F(2) - A26 - A610 - (IA10 + IS10) \qquad (6\text{-}2)$$

where the expression in parentheses is identical to the instantaneous absorbed insolation of earth given by the numerator of (4-37).

The net terrestrial flux F_2^* was derived in Eq. (3-11) and was not subject to any systematic diurnal variation. Thus F_2^* may be taken as constant for a 24-hour period.

Note that the first symbol at k=2 in Fig. 6 is not F(2), but QAVE, defined for each gridpoint by the analog of (4-1), namely

$$QAVE = S\left(\frac{r}{r_m}\right)^{-2} \overline{\overline{\overline{\overline{Cos\ Z}}}} \qquad (6\text{-}3)$$

Here $\overline{\overline{\overline{\overline{Cos\ Z}}}}$ is the 24-hour average of Cos Z, and is given by

$$\overline{\overline{\overline{\overline{Cos\ Z}}}} = [H\ Sin\ \phi\ Sin\ \delta + Cos\ \phi\ Cos\ \delta\ Sin\ H]/\pi \qquad (6\text{-}4)$$

where

$$H = arc\ Cos\ [-Tan\ \phi\ Tan\ \delta] \qquad (6\text{-}5)$$

is the hour angle from local noon to sunset at the gridpoint. Thus the instantaneous values of incident insolation and of reflected insolation have been converted from F(2) and REF to their 24-hour averages denoted by

$$QAVE = F(2)\ \overline{\overline{\overline{\overline{Cos\ Z}}}}/Cos\ Z \qquad (6\text{-}6)$$

and

$$QREF = REF\ \overline{\overline{\overline{\overline{Cos\ Z}}}}/Cos\ Z \qquad (6\text{-}7)$$

respectively.

The reason for the conversion in (6-6) and (6-7) is to convert the net incoming insolation at k=2 to values that are comparable in time-scale to those of F_2*. This device has the advantage of showing whether the resultant averaged heat-transfer quantities are compatible with the expected approximation to a heat budget for the given date. However, if it were desired to exhibit the expected diurnal variation of heat-transfers across the layers (2,6), (6,10) and at the ground, the quantity QAVE and all other solar-heating rates to be discussed would be multiplied by the factor

$$(\text{Cos } Z/\overline{\overline{\text{Cos } Z}})$$

assuming that all the layer absorptivities and the solar reflectivity are constant during the day for which the diurnal variation of heat transfers are of interest.

With the solar quantities averaged for the day, one obtains

$$\text{BALT} = \text{QAVE} - (\text{QREF} + F_2^*) \qquad (6\text{-}8)$$

as a 24-hour average radiational balance in cal cm^{-2} min^{-1} for the tropopause.

C. CROSS-SECTIONAL RADIATIVE TRANSFERS IN LAYER (2,6)

At this layer, in Fig. 6, the heat-transfers are assumed, as in the FNWC heating model, to be radiative only. For convenient comparison with climatology, the heating (cooling) rate is given by

$$\text{BAL26} = \text{Q26} - \text{F26} \qquad (6\text{-}9)$$

where Q26 is the daily average absorption in layer (2,6) and is defined relative to A26 by an equation analogous to Eq. (6-6). The terrestrial cooling rate F26 is defined by Eq. (3-12a).

Note that all values of BAL26 were negative in all cross-sectional diagrams, Figs. 7,...,10.

D. CROSS-SECTIONAL DATA FOR LAYER (6,10)

1. Radiative Transfers Only

Neglecting temporarily the turbulent transfers at the earth-air interface, the present heating model computes the 24-hour average radiative cooling computed by the difference equation

$$BAL610 = Q610 - F610 \qquad (6\text{-}10)$$

in a manner analogous to Eq. (6-9). The parameter BAL610 was negative at all gridpoints of Figs. 7,...,10. In fact the ratio R = F610/Q610 varied with latitude as follows

	0°	10°	20°	30°	40°	50°	60°
R =	1.916	2.219	2.577	2.893	3.912	4.122	4.903

Even when the instantaneous (near-noon) radiation balance was considered, the difference remained at least slightly negative in low latitudes corresponding to cooling. In higher latitudes, instantaneous cooling rates were never reversed by consideration of the instantaneous computation of the radiation balance in layer (6,10).

2. Heat Balance at the Earth's Surface

In Section V.B, the earth-to-air turbulent transfer of latent heat, E, has been modeled after Kaitala (1974), through Eq. (5-1). The sensible heat transfer, H_Γ, given by

$$H_\Gamma = rE$$

where r is the Bowen ratio determined empirically by Eq. (5-5) as a function of latitude.

The sum of the turbulent heat transfers, $H_\Gamma+E$, has been subtracted from the average radiation at the earth's surface

$$R = QABG - F_{10}* \tag{6-11}$$

to form the average warming rate, BALB, at the surface

$$BALB = QABG - F_{10}* - (H_\Gamma+E) \tag{6-12}$$

where QABG is related to ABG of Eq. (4-37) by an analog to Eq. (6-6) and $F_{10}*$ is defined by Eq. (3-10) which is taken as constant for a 24-hour period as was the case with F_2*.

The parameter BALB has been shown in each cross-section as a function first of gridpoint on each meridian, and subsequently interpolated to 5° latitude increments as indicated in connection with Eq. (6-1).

3. Sensible Heat Modification of the Atmospheric Columns

In Figs. 7,...,10 the sensible heat transfer, H_Γ, which crosses the earth-air interface has been added to the air only in the layer (8,10), (cf. Kaitala, 1974). In this connection, the net radiative loss in the layer (6,10) has

been subdivided equally into two halves, BAL68 and BAL810 (excluding H_Γ), equal to half the radiative loss BAL610.

The sensible heat transfer H_Γ, which has been allowed to diffuse only into layer (8,10), is shown as item (n) of layer (8,10) in Fig. 6. In the numerical computations, H_Γ is the smallest of all the heat-transfers considered in any atmospheric column presented in Figs. 7,...,10.

E. MERIDIONAL CROSS-SECTIONS OF THE VERTICAL HEAT BUDGET

Note that the single-time set of heating computations for each of the four meridians, 125°W, 170°W, 145°E, and 35°W, are shown in Figs. 7,...,10 respectively. These figures show the individual computations of the warming and cooling which are schematically formatted in Fig. 6, together with the layers to which they contribute in the heating model.

Note also that the four meridional cross-sections depicted each have two sections: section (a) depicts results for a "tropical" section with gridpoints extending from 20°S (or the southernmost latitude to which the meridian in question extends) to 25°N, while section (b) of Figs. 7,...,10 depicts the gridpoint computations (averaged for 24-hours) over the latitudinal range 30°N to 65°N (or the northernmost latitude to which the meridian in question extends). Recall the latitudinal boundaries for the selected meridians were required to remain over the ice-free ocean on the FNWC grid.

The latitudinal variation of both the short- and long-wave calculations, as observed in Figs. 7,...,10, seem to

have uniform gradients across each meridian in spite of the differing climatic zones represented. Hence it was reasonable to formulate a mean radiational balance model for 16 October 1973, which is presented in Section VII.

k			
	LAT.		latitude of the gridpoints in 5° increments
	a)	QAVE	24-hour averaged insolation at level k=2
	b)	QREF	Reflected average insolation at level k=2
	c)	F_2*	Net Outgoing long-wave flux at level k=2
2	d)	BALT	averaged earth-tropospheric gain or loss (a-b-c)
	e)	Q26	averaged solar insolation absorbed by layer (2,6), positive heating
	f)	F26	IR flux loss by layer (2,6)
	g)	BAL26	averaged radiative cooling in layer (2,6) (e-f)
6	h)	(CL)	total opaque cloud amount, by Eq. (4-44)
	i)	Q68	averaged solar insolation absorbed by layer (6,8)
	j)	F68	IR flux loss by layer (6,8)
	k)	BAL68	averaged radiative cooling in layer (6,8) (i-j)
8			
	l)	Q810	averaged solar insolation absorbed by layer (8,10)
	m)	F810	IR flux loss by layer (8,10)
	n)	H_Γ	sensible heat gain in layer (8,10)
	o)	BAL810	averaged heat balance in layer (8,10) (l-m+n)
10			
	p)	QABG	averaged solar insolation absorbed by surface
	q)	F_{10}*	net long-wave flux at earth's surface
	r)	$E+H_\Gamma$	combined heat loss due to evaporation and sensible heat transport
	s)	BALB	averaged warming or cooling at earth's surface (p-q-r)

Figure 6. Key to Meridional cross-sections for Figs. 7,...,10. All radiative and turbulent transfer values are in cal cm^{-2} min^{-1} for the levels or layers considered.

LAT.	-20.0	-15.0	-10.0	-5.0	0.0	5.0	10.0	15.0	20.0	25.0
2	0.6265	0.6306	0.6300	0.6248	0.6149	0.6005	0.5816	0.5583	0.5309	0.4996
	0.3308	0.3247	0.3034	0.2668	0.2592	0.2320	0.2475	0.2277	0.1799	0.1383
	0.2835	0.2854	0.2909	0.2940	0.2931	0.2953	0.2921	0.3024	0.3203	0.3462
	0.0120	0.0204	0.0357	0.0641	0.0627	0.0731	0.0420	0.0282	0.0308	0.0151
	0.0664	0.0693	0.0702	0.0705	0.0705	0.0699	0.0698	0.0640	0.0549	0.0427
	0.1392	0.1413	0.1404	0.1388	0.1404	0.1307	0.1358	0.1300	0.1155	0.0957
	-0.0730	-0.0720	-0.0703	-0.0683	-0.0699	-0.0609	-0.0660	-0.0660	-0.0606	-0.0529
6	(0.89)	(0.87)	(0.81)	(0.71)	(0.70)	(0.62)	(0.71)	(0.64)	(0.41)	(0.15)
	0.0307	0.0299	0.0283	0.0246	0.0237	0.0198	0.0209	0.0213	0.0193	0.0177
	0.0399	0.0439	0.0472	0.0451	0.0472	0.0383	0.0374	0.0425	0.0484	0.0602
	-0.0092	-0.0140	-0.0189	-0.0205	-0.0235	-0.0185	-0.0164	-0.0212	-0.0291	-0.0425
8	0.0307	0.0299	0.0283	0.0246	0.0237	0.0198	0.0209	0.0213	0.0193	0.0177
	0.0399	0.0439	0.0472	0.0451	0.0472	0.0383	0.0374	0.0425	0.0484	0.0602
	0.0110	0.0030	0.0014	0.0009	0.0005	0.0014	0.0021	0.0021	0.0012	0.0020
	0.0022	-0.0109	-0.0175	-0.0197	-0.0230	-0.0170	-0.0143	-0.0191	-0.0279	-0.0405
10	0.1681	0.1767	0.1998	0.2335	0.2377	0.2590	0.2224	0.2239	0.2576	0.2830
	0.0647	0.0562	0.0561	0.0649	0.0581	0.0880	0.0816	0.0875	0.1080	0.1299
	0.1689	0.0533	0.0229	0.0120	0.0049	0.0197	0.0349	0.0354	0.0191	0.0239
	-0.0658	0.0672	0.1208	0.1615	0.1747	0.1513	0.1058	0.1010	0.1306	0.1292

Figure 7(a). 125°W Longitudinal cross-section, tropical section. Refer to Fig. 6 for key. Values computed from data for 16 October 1973.

LAT.	30.0	35.0	40.0	45.0	50.0	55.0
2	0.4646	0.4263	0.3848	0.3407	0.2942	0.2459
	0.1184	0.1161	0.1274	0.1206	0.1491	0.1112
	0.3769	0.3799	0.3265	0.3209	0.2915	0.2295
	-0.0307	-0.0698	-0.0691	-0.1009	-0.1464	-0.0948
	0.0325	0.0275	0.0323	0.0284	0.0242	0.0265
	0.0871	0.0876	0.0981	0.1031	0.1130	0.0928
	-0.0546	-0.0602	-0.0657	-0.0746	-0.0888	-0.0664
6	(0.0)	(0.0)	(0.17)	(0.20)	(0.76)	(0.56)
	0.0166	0.0158	0.0118	0.0140	0.0185	0.0049
	0.0703	0.0753	0.0579	0.0520	0.0607	0.0260
	-0.0538	-0.0595	-0.0461	-0.0380	-0.0422	-0.0210
8	0.0166	0.0158	0.0118	0.0140	0.0185	0.0049
	0.0703	0.0753	0.0579	0.0520	0.0607	0.0260
	0.0052	0.0056	0.0039	0.0117	0.0097	-0.0030
	-0.0485	-0.0539	-0.0422	-0.0263	-0.0324	-0.0240
10	0.2807	0.2510	0.2014	0.1635	0.0837	0.0983
	0.1491	0.1415	0.1125	0.1140	0.0570	0.0847
	0.0479	0.0407	0.0233	0.0558	0.0409	-0.0108
	0.0836	0.0688	0.0656	-0.0062	-0.0142	0.0244

Figure 7(b). 125°W Longitudinal cross-section, higher latitude section. Refer to Fig. 6 for key. Values computed from data for 16 October 1973.

LAT.	30.0	35.0	40.0	45.0	50.0	55.0	60.0	65.0
	0.4646	0.4262	0.3848	0.3407	0.2942	0.2459	0.1963	0.1459
	0.2063	0.2378	0.1941	0.1354	0.0973	0.1050	0.0982	0.0861
	0.3518	0.2960	0.3784	0.2967	0.2720	0.2137	0.2157	0.1710
2	-0.0935	-0.1076	-0.1878	-0.0914	-0.0750	-0.0728	-0.1177	-0.1111
	0.0336	0.0380	0.0153	0.0263	0.0266	0.0311	0.0259	0.0217
	0.1187	0.1359	0.0912	0.1012	0.1085	0.1166	0.1381	0.1305
	-0.0851	-0.0980	-0.0759	-0.0749	-0.0819	-0.0855	-0.1122	-0.1089
6	(0.77)	(0.97)	(0.90)	(0.58)	(0.38)	(0.72)	(0.88)	(1.00)
	0.0298	0.0256	0.0296	0.0142	0.0069	0.0034	0.0046	0.0035
	0.0812	0.0587	0.1188	0.0632	0.0361	0.0123	0.0180	0.0107
	-0.0514	-0.0331	-0.0893	-0.0490	-0.0291	-0.0089	-0.0135	-0.0071
8								
	0.0298	0.0256	0.0296	0.0142	0.0069	0.0034	0.0046	0.0035
	0.0812	0.0587	0.1188	0.0632	0.0361	0.0123	0.0180	0.0107
	0.0178	0.0134	0.0154	0.0058	0.0052	0.0363	0.0116	0.0059
	-0.0335	-0.0198	-0.0739	-0.0433	-0.0239	0.0273	-0.0019	-0.0012
10								
	0.1650	0.0992	0.1163	0.1507	0.1566	0.1030	0.0629	0.0312
	0.0707	0.0425	0.0497	0.0691	0.0915	0.0725	0.0415	0.0192
	0.1625	0.0958	0.0901	0.0279	0.0225	0.1356	0.0394	0.0188
	-0.0682	-0.0390	-0.0234	0.0537	0.0427	-0.1051	-0.0180	-0.0069

Figure 8(b). 170°W Longitude cross-section, higher latitude section. Refer to Fig. 6 for key. Values computed from data for 16 October 1973.

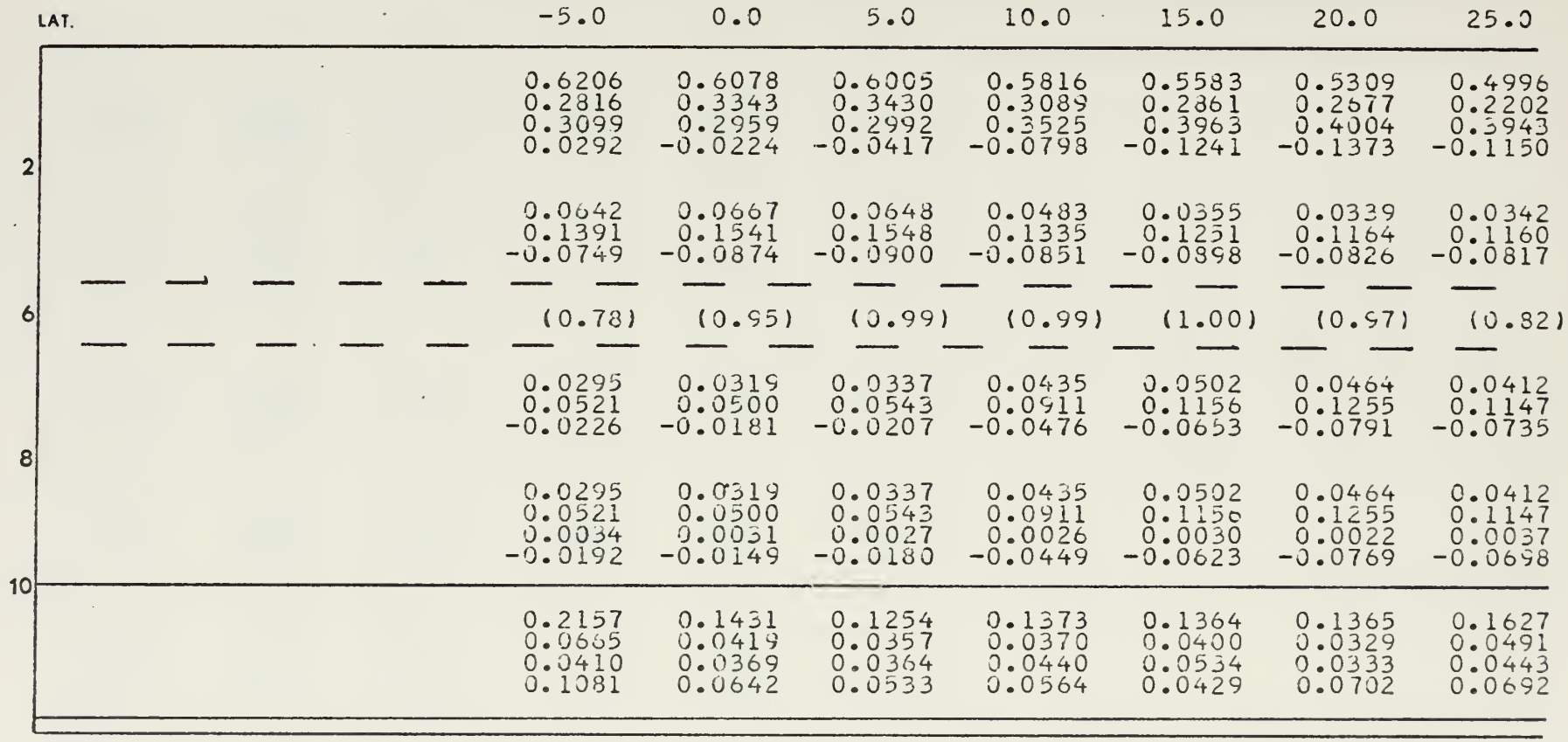

Figure 9(a). 145°E Longitudinal cross-section, tropical section. Refer to Fig. 6 for key. Values computed from data for 16 October 1973.

LAT.	30.0	35.0	40.0	45.0	50.0	55.0
2	0.4646	0.4263	0.3848	0.3407	0.2942	0.2459
	0.2386	0.1848	0.0874	0.1387	0.1108	0.1454
	0.3876	0.3913	0.3971	0.3362	0.3159	0.2731
	-0.1617	-0.1498	-0.0998	-0.1343	-0.1325	-0.1727
	0.0293	0.0188	0.0132	0.0168	0.0175	0.0175
	0.1213	0.1063	0.0800	0.0877	0.0891	0.1064
	-0.0920	-0.0875	-0.0668	-0.0709	-0.0716	-0.0889
6	(1.00)	(0.70)	(0.03)	(0.54)	(0.38)	(1.00)
	0.0420	0.0305	0.0132	0.0176	0.0124	0.0180
	0.1148	0.0858	0.0610	0.0582	0.0539	0.0609
	-0.0728	-0.0553	-0.0477	-0.0406	-0.0415	-0.0429
8	0.0420	0.0305	0.0132	0.0176	0.0124	0.0180
	0.1148	0.0858	0.0610	0.0582	0.0539	0.0609
	0.0174	0.0643	0.0739	0.0871	0.0546	0.0457
	-0.0553	0.0090	0.0262	0.0465	0.0131	0.0029
10	0.1127	0.1618	0.2577	0.1499	0.1409	0.0471
	0.0368	0.1135	0.1952	0.1320	0.1189	0.0451
	0.1489	0.4632	0.4276	0.4205	0.2294	0.1721
	-0.0729	-0.4148	-0.3651	-0.4026	-0.2074	-0.1700

Figure 9(b). 145°E Longitudinal cross-section, higher latitude section. Refer to Fig. 6 for key. Values computed from data for 16 October 1973.

LAT.	-20.0	-15.0	-10.0	-5.0	0.0	5.0	10.0	15.0	20.0	25.0
	0.6265	0.6306	0.6300	0.6248	0.6149	0.6005	0.5816	0.5583	0.5309	0.4996
	0.2751	0.2830	0.2852	0.2645	0.2549	0.1571	0.1468	0.1367	0.1552	0.1647
	0.2910	0.2931	0.2964	0.2988	0.2999	0.3886	0.3638	0.3500	0.3629	0.3797
2	0.0600	0.0544	0.0484	0.0616	0.0603	0.0548	0.0710	0.0715	0.0128	-0.0448
	0.0646	0.0673	0.0683	0.0677	0.0665	0.0433	0.0476	0.0477	0.0415	0.0349
	0.1357	0.1411	0.1447	0.1396	0.1405	0.1061	0.1136	0.1139	0.1089	0.1039
	-0.0713	-0.0738	-0.0764	-0.0719	-0.0738	-0.0629	-0.0660	-0.0662	-0.0675	-0.0690
6	(0.76)	(0.78)	(0.79)	(0.74)	(0.73)	(0.36)	(0.34)	(0.33)	(0.42)	(0.50)
	0.0253	0.0264	0.0269	0.0250	0.0243	0.0330	0.0261	0.0217	0.0266	0.0306
	0.0412	0.0462	0.0497	0.0391	0.0433	0.0885	0.0682	0.0571	0.0755	0.0920
	-0.0158	-0.0198	-0.0228	-0.0141	-0.0191	-0.0555	-0.0421	-0.0355	-0.0489	-0.0613
8										
	0.0253	0.0264	0.0269	0.0250	0.0243	0.0330	0.0261	0.0217	0.0266	0.0306
	0.0412	0.0462	0.0497	0.0391	0.0433	0.0885	0.0682	0.0571	0.0755	0.0920
	0.0045	0.0014	0.0008	0.0032	0.0031	0.0025	0.0027	0.0031	0.0037	0.0056
	-0.0112	-0.0184	-0.0221	-0.0109	-0.0160	-0.0528	-0.0394	-0.0323	-0.0452	-0.0558
10										
	0.2358	0.2274	0.2228	0.2426	0.2449	0.3340	0.3349	0.3304	0.2810	0.2387
	0.0732	0.0597	0.0522	0.0808	0.0727	0.1055	0.1138	0.1219	0.1029	0.0917
	0.0686	0.0236	0.0147	0.0452	0.0313	0.0347	0.0448	0.0542	0.0565	0.0666
	0.0938	0.1442	0.1557	0.1166	0.1410	0.1939	0.1762	0.1542	0.1216	0.0803

Figure 10(a). 35°W Longitudinal cross-section, tropical section. Refer to Fig. 6 for key. Values computed from data for 15 October 1973.

LAT.	30.0	35.0	40.0	45.0	50.0	55.0	60.0
	0.4646	0.4263	0.3848	0.3407	0.2942	0.2459	0.1962
	0.2109	0.2115	0.1767	0.1301	0.1399	0.1033	0.0857
	0.3163	0.2658	0.2780	0.3803	0.3694	0.3325	0.2961
	-0.0626	-0.0510	-0.0699	-0.1697	-0.2152	-0.1898	-0.1855
2							
	0.0442	0.0499	0.0405	0.0176	0.0107	0.0155	0.0151
	0.1280	0.1463	0.1299	0.1050	0.0924	0.1030	0.0961
	-0.0838	-0.0964	-0.0894	-0.0874	-0.0817	-0.0875	-0.0810
6	(0.76)	(0.85)	(0.75)	(0.46)	(0.74)	(0.52)	(0.46)
	0.0240	0.0158	0.0158	0.0197	0.0229	0.0153	0.0098
	0.0589	0.0270	0.0377	0.0860	0.0998	0.0727	0.0526
	-0.0349	-0.0111	-0.0218	-0.0664	-0.0769	-0.0574	-0.0429
8							
	0.0240	0.0158	0.0158	0.0197	0.0229	0.0153	0.0098
	0.0589	0.0270	0.0377	0.0860	0.0998	0.0727	0.0526
	0.0090	0.0113	0.0132	0.0212	0.0721	0.0150	0.0409
	-0.0259	0.0002	-0.0087	-0.0453	-0.0047	-0.0424	-0.0020
10							
	0.1614	0.1333	0.1359	0.1537	0.0977	0.0964	0.0758
	0.0704	0.0657	0.0727	0.1033	0.0775	0.0840	0.0946
	0.0821	0.0808	0.0766	0.1030	0.3017	0.0550	0.1454
	0.0089	-0.0132	-0.0134	-0.0525	-0.2814	-0.0427	-0.1641

Figure 10(b). 35°W Longitudinal cross-section, higher latitude section. Refer to Fig. 6 for key. Values computed from data for 15 October 1973.

VII. MEAN BUDGETARY BALANCE MODEL

By averaging key parameters, discussed in Section VI, across the four possible meridional lines at each 5° latitude increment from 0° to 65°N, a mean heat budget model was constructed which may be considered representative of Fall in the annual cycle. The advantage of such averaging is to facilitate the comparisons of this study's results with other published heat budget results (cf. Budyko, 1956) even though such results are generally annual means. Also, by averaging over the four meridians studied here, meridional differences tend to be smoothed out, so that the zonally-averaged heat budgets of this study may be compared with others in the literature.

A. RADIATION MODEL OF THE OCEAN-ATMOSPHERE SYSTEM

Fig. 11(a) depicts the schematic format of the mean radiation meridional cross-section (Figs. 11(b) and (c)). Turbulent transfer parameters have been omitted from this display and only Northern Hemisphere values are given.

Note that the radiational quantities for the layers (6,8) and (8,10) of Figs. 7,...,10 have been combined at identical latitudes in Fig. 11 as for the layer (6,10) and that all resultant values are meridionally averaged where possible. Since only the 170°W meridian contains results at 65°N, the value at this latitude is not representative of the zonal-averaging process described above.

k			
	LAT		latitude of the gridpoints in 5°increments
	a)	$\overline{QAVE}$	24-hour averaged mean insolation at level k=2
	b)	$\overline{QREF}$	mean reflected average insolation at level k=2
	c)	$\overline{F_2*}$	mean net outgoing long-wave flux at level k=2
2	d)	$\overline{BALT}$	mean averaged earth-tropospheric gain rate (a-b-c)
	e)	$\overline{Q26}$	mean averaged solar insolation absorbed by layer (2,6)
	f)	$\overline{F26}$	mean IR flux loss by layer (2,6)
	g)	$\overline{BAL26}$	mean averaged radiative cooling rate, layer (2,6) (e-f)
6	h)	$\overline{Q610}$	mean averaged solar insolation absorbed by layer (6,10)
	i)	$\overline{F610}$	mean IR flux loss by layer (6,10)
	j)	$\overline{BAL610}$	mean averaged radiative cooling rate, layer (6,10) (h-i)
10	k)	$\overline{QABG}$	mean averaged solar insolation absorbed by surface
	l)	$\overline{F_{10}*}$	mean net long-wave flux at earth's surface
	m)	$\overline{BAL10}$	mean averaged radiational warming (cooling) rate at earth's surface (k-l)

Figure 11(a). Key to mean radiation meridional cross-section for Figs. 11(b) and (c). All radiational values have been averaged over a 24-hour day and are expressed in cal cm^{-2} min^{-1} for the levels or layers considered. The over-bar symbol refers to mean values averaged over the possible meridional lines (125°W, 170°W, 145°E, and 35°W).

LAT	0.0	5.0	10.0	15.0	20.0	25.0	30.0
k	.6131	.6005	.5816	.5583	.5309	.4996	.4646
	.2579	.2334	.2283	.2183	.2108	.1894	.1936
	.3092	.3313	.3399	.3460	.3554	.3722	.3581
2	.0456	.0358	.0134	-.0060	-.0353	-.0620	-.0871
	.0636	.0572	.0530	.0483	.0432	.0363	.0349
	.1379	.1278	.1253	.1234	.1164	.1069	.1138
	-.0743	-.0706	-.0723	-.0751	-.0732	-.0706	-.0789
6	.0533	.0570	.0607	.0616	.0622	.0630	.0562
	.1021	.1225	.1347	.1387	.1603	.1820	.1626
	-.0488	-.0655	-.0740	-.0771	-.0981	-.1190	-.1064
10	.2378	.2530	.2395	.2302	.2148	.2109	.1799
	.0691	.0810	.0799	.0839	.0787	.0833	.0817
	.1687	.1720	.1596	.1463	.1361	.1276	.0982

Figure 11(b). Mean radiation meridional cross-section for tropical latitudes. Refer to Fig. 11(a) for key. All values listed are in cal cm^{-2} min^{-1} and are computed from data for 16 October 1973.

LAT	35.0	40.0	45.0	50.0	55.0	60.0	65.0
k	.4263	.3848	.3407	.2942	.2459	.1962	.1459
	.1875	.1464	.1312	.1243	.1162	.0920	.0861
	.3332	.3450	.3335	.3122	.2622	.2559	.1710
2	-.0944	-.1066	-.1240	-.1423	-.1325	-.1517	-.1112
	.0336	.0253	.0223	.0197	.0227	.0205	.0217
	.1190	.0998	.0992	.1007	.1047	.1171	.1305
	-.0854	-.0745	-.0769	-.0810	-.0820	-.0966	-.1089
6	.0438	.0352	.0328	.0304	.0208	.0144	.0070
	.1234	.1377	.1297	.1253	.0860	.0706	.0214
	-.0796	-.1025	-.0969	-.0949	-.0652	-.0562	-.0144
10	.1613	.1778	.1545	.1197	.0862	.0694	.0312
	.0908	.1075	.1046	.0862	.0716	.0681	.0192
	.0705	.0703	.0499	.0335	.0146	.0013	.0120

Figure 11(c). Mean radiation meridional cross-section for mid-latitudes. Refer to Fig. 11(a) for key. All values listed are in cal cm^{-2} min^{-1} and are computed from data for 16 October 1973.

To facilitate a graphical display of the results contained in Fig. 11 and for ease of comparison with published yearly climatological results (Malkus, 1962), the model displayed in Fig. 11 has been used as the basis for testing the following component heat balances: (a) the earth-atmosphere system balance (using symbols consistent with Malkus (1962)), (b) the atmospheric radiative balance, and (c) the earth-surface balance.

B. RADIATION BALANCES OF THE OCEAN-TROPOSPHERE SYSTEM

The first graph, Fig. 12, consists of a radiation balance composed of three parameters, R_s, R_a, and R, which are defined (after Malkus, 1962) as follows: (1) R_s is mean radiative energy gain (loss) rate of the ocean-troposphere system which was referred to as $\overline{BALT}$ at k=2 in Fig. 11(a); (2) R_a is the mean radiative cooling rate in the troposphere which is defined as the sum of $\overline{BAL26}$ and $\overline{BAL610}$ from Fig. 11(a); and (3) R, the mean radiative warming (cooling) rate at the earth's surface which was identified as $\overline{BAL10}$ in Fig. 11(a). The relationship between the three radiative parameters can be expressed as

$$R_s = R + R_a \qquad (7\text{-}1)$$

Table III lists quantitative comparisons of R_s, R_a, and R, as found in this study for 16 October 1973, with values reported in Malkus (1962) for the climatological year, and values reported by Jenks (1974) for 25 April 1973. The latitudinally-averaged values are obtained by weighting each value by the cosine of the latitude

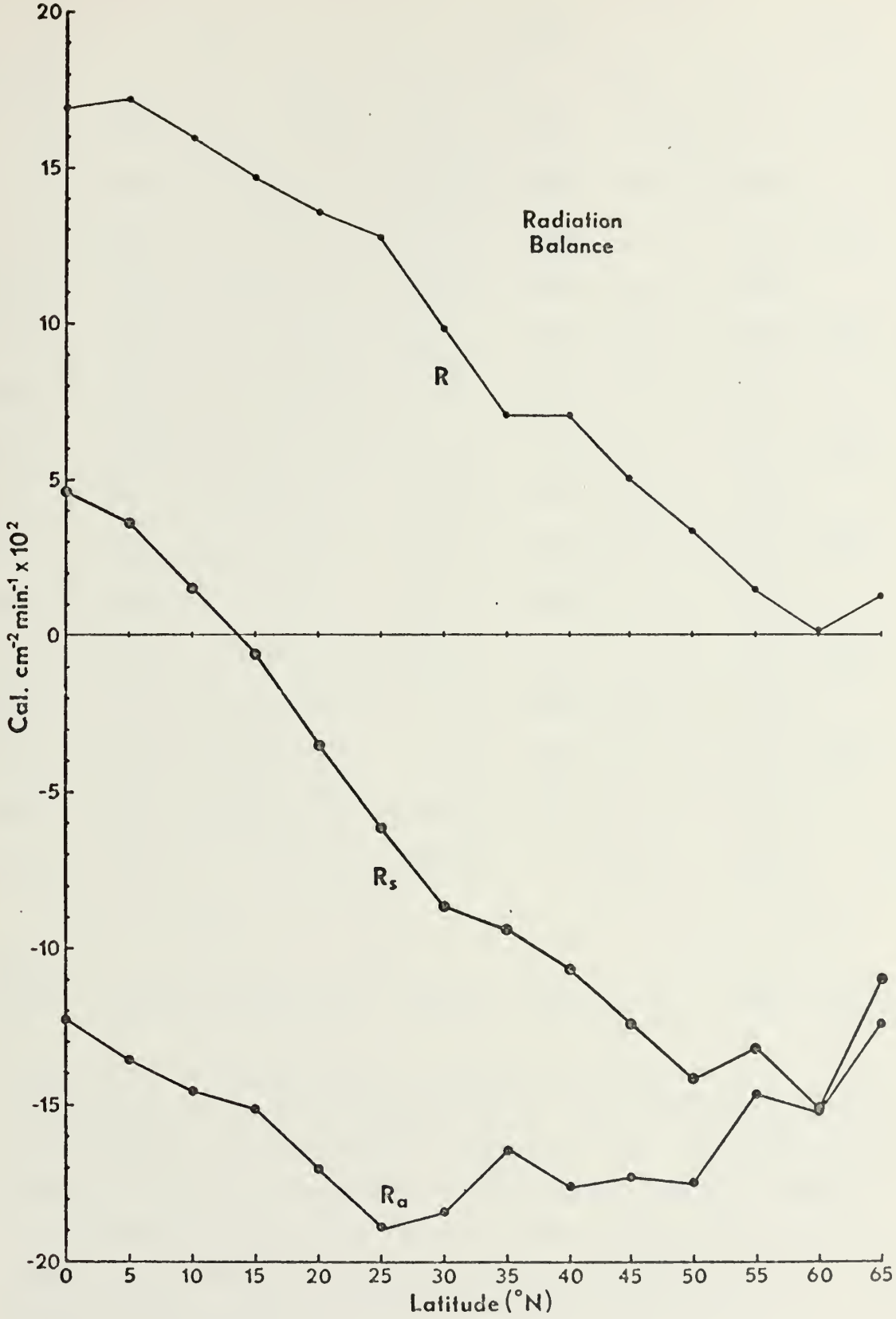

Figure 12. Radiational balance at the tropopause (R_s); in the atmospheric column between k=2 and k=10 (R_a); and at the surface (R) for 16 October 1973.

	(a)	(b)	(c)
°LAT	R_{s_1} / R_{s_2} / R_{s_3}	R_{a_1} / R_{a_2} / R_{a_3}	R_1 / R_2 / R_3
0	.0456/.0627/.031	-.1231/-.1235/-.132	.1687/ /.154
5	.0358/.0608/.024	-.1361/-.1254/-.142	.1720/.2033/.158
10	.0149/.0589/.032	-.1463/-.1292/-.167	.1596/ /.194
15	-.0060/.0513/.041	-.1522/-.1387/-.167	.1463/.2090/.208
20	-.0353/.0437/.032	-.1713/-.1368/-.179	.1361/ /.206
25	-.0620/.0361/.062	-.1896/-.1235/-.174	.1276/.1900/.236
30	-.0871/.0266/.068	-.1853/-.1178/-.160	.0982/ /.225
35	-.0944/.0171/.055	-.1650/-.1102/-.153	.0705/.1482/.201
40	-.1066/ 0.0 /.044	-.1770/-.1159/-.140	.0703/ /.175
45	-.1240/-.0418/-.003	-.1738/-.1273/-.135	.0499/.1026/.132
50	-.1423/-.0570/.009	-.1759/-.1330/-.128	.0336/ /.124
55	-.1325/-.0684/.022	-.1472/-.1330/-.132	.0146/.0646/.155
60	-.1517/-.0760/.042	-.1528/-.1311/-.141	.0013/ /.184
65N	-.1112/ /.106	-.1233/ /-.114	.0120/ /.219
Wt. Avg.	-.0552/.0186/.039	-.1589/-.1264/-.150	.1037/.1625/.185

Table III. Comparisons of Radiational Balances (a) at the tropopause R_s, (b) in the vertical column R_a between k=2 and k=10, and (c) at the earth's surface R of the meridionally averaged values as found in this study denoted by subscript "1". The corresponding annual values reported by Malkus (1962) are denoted by subscript "2", and those for 25 April 1973 found by Jenks (1974) denoted by subscript "3". All values are in ly min^{-1}.

$$\text{Wt. Avg.} = \frac{\sum_{i=1}^{n} Q_i \cos \phi_i}{\sum_{i=1}^{n} \cos \phi_i} \qquad (7\text{-}2)$$

It can be noted from Table III that although the R_s values found by this study are consistently lower than those reported by Malkus for the year, the seasonally higher values reported by Jenks tend to offset this difference. The same holds true for the balance at the surface (R). However, both seasonal studies show greater radiative cooling in the troposphere (R_a) than the yearly climatological values which evidently was obtained after Budyko (1956) as a residual between R_s and R, as functions of latitude. It is noteworthy that Jenks' (1974) R_s results (column (c) of Table III) are greater than those obtained here by .094 ly min^{-1} (in the mean), and of this surplus the additional heating rate $\Delta R = 0.081$ ly min^{-1} is found at the surface.

C. TROPOSPHERIC HEATING

Fig. 13 graphically depicts the mean tropospheric heat budget as found in this study. The parameters presented include: R_a which was discussed in Sec. VII.B, $(E+H_\Gamma)$ which is the turbulent heat transfer rate due to latent and sensible heat transport realized in the atmosphere, Q_{va} which is the net heat flux divergence rate in the troposphere required to bring about a heat balance (which would not be expected to be achieved for the time scale here), and S_a the storage term. These terms are related by

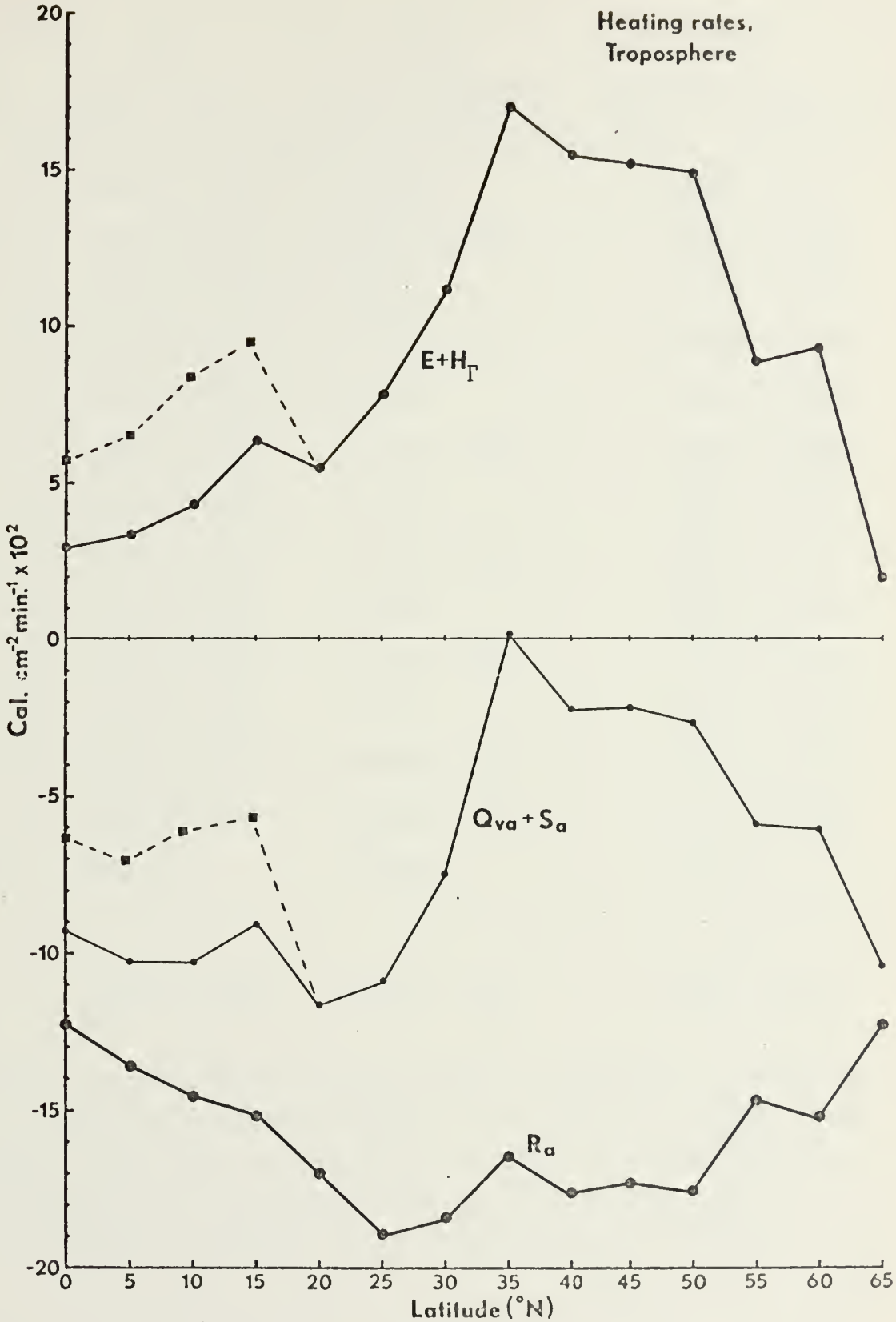

Figure 13. Tropospheric Heat Budget Disposition. The net heat loss in the Troposphere ($Q_{va}+S_a$) is depicted as the sum of the tropospheric radiative cooling (R_a) and the turbulent transfer heating ($E+H_\Gamma$) in the troposphere.

°LAT	(a) R_{a_1} / R_{a_2}	(b) $(E+H_\Gamma)_1/(E+H_\Gamma)_2$	(c) $(Q_{va}+S_a)_1/(Q_{va}+S_a)_2$
0	-.1231/-.1235	.0294/	-.0937/ .0874
5	-.1361/-.1254	.0332/.1539	0.1029/ .0285
10	-.1463/-.1297	.0425/	-.1038/ .0437
15	-.1522/-.1387	.0636/.1786	-.0916/ .0095
20	-.1713/-.1368	.0544/	-.1169/-.0057
25	-.1896/-.1235	.0744/.1748	-.1095/-.0095
30	-.1853/-.1178	.1164/	-.0749/ .0190
35	-.1650/-.1102	.1701/.1615	-.0051/ .0190
40	-.1770/-.1159	.1544/	-.0226/ .0038
45	-.1738/-.1273	.1518/.1254	-.0220/-.0095
50	-.1759/-.1330	.1486/	-.0273/-.0152
55	-.1472/-.1330	.0880/.0988	-.0592/-.0228
60	-.1528/-.1311	.0924/	-.0604/-.0266
65N	-.1233/	.0188/	-.1045/
Wt Avg.	-.1589/-.1264	.0855/.1533	-.0735/ .0201

Table IV. Comparisons of trapospheric radiative cooling rate (R_a), turbulent transport warming rate ($E+H_\Gamma$), and net tropospheric heat loss rate ($Q_{va}+S_a$) as found by this study for 16 October 1973 denoted by subscript "1" and as reported by Malkus (1962) for yearly climatology denoted by subscript "2".

$$Q_{va} + S_a = R_a + (E+H_\Gamma) \qquad (7\text{-}3)$$

The storage rate S_a has not been separated specifically from Q_{va}, but over the annual cycle it is assumed zero. Assuming, however that $Q_{va}=0$, if the weighted average values from Table IV are set into Eq. (7-3), to determine the mean storage cooling rate, S_a, the latter turns out to be

$$\overline{S_a} \equiv \left(\frac{\overline{\partial T}}{\partial t}\right)_a = -.54°C\ (day)^{-1}$$

for the time (16 October 1973) under study. The net lateral flux-divergence term Q_{va} has not been assessed here, but presumably its mean effect would show up as cold advection across the equator, and would result in a reduced value of $\overline{S_a}$.

In Fig. 13, the dashed portion of the $(E+H_\Gamma)$ and $(Q_{va}+S_a)$ curves are displayed to show the effects of varying the K* value in the calculation of latent heat transport (Eq. 5-1), as discussed in Section V. In the dashed portion, the K* value of 2×10^5 cm^2 sec^{-1} was tested for latitudes 0°, 5°, and 10°N, with a transitional value of 1.5×10^5 cm^2 sec^{-1} used at 15°N. At all points on the solid $(E+H_\Gamma)$ line K* was 1×10^5 cm^2 sec^{-1}. This smaller K* value seemed to provide more realistic values of $(E+H_\Gamma)$ in mid-latitudes but to somewhat unrealistically small values in low latitudes.

A possible explanation for the small $(E+H_\Gamma)$ values at low latitudes is the difficulty in correctly determining the temperature and humidity gradients between the surface and the top of the constant flux layer in the data-sparse

equatorial areas. In these tropical latitudes some time- and space-smoothing of the few available radiosondes could have been introduced into the original FNWC map analyses, which would tend to smooth out vertical gradients as against those to be expected with observed radiosondes on 16 October 1973. Hence it was considered justifiable to revert to Kaitala's (1974) suggested $K^* = 2 \times 10^5$ cm^2 sec^{-1} in low latitudes, 0°-10°N, where the resultant dashed $(E+H_\Gamma)$ curve of Fig. 13 qualitatively appears more reasonable. For example, the peak in $(E+H_\Gamma)$ at 15°N appears to be due to relatively strong evaporative and sensible heat transfers associated with the Trade Wind regime, while the higher latitude peak (35°-50°N) in Fig. 13 is due to the trend towards winter maximum turbulent-heat transfers associated with cool continental air flowing over warm ocean currents.

No attempt to select a final K* value is suggested from these results. If the same turbulent-transfer model can be tested over a large enough set of seasonal samples, it should be possible to assess the appropriate K*-value which yields the best approximation to the atmospheric heat balance.

D. SURFACE HEATING RATES

Fig. 14 depicts the zonally-averaged surface heating budget as a function of latitude resulting from this study. The parameters include the net surface radiative warming (R), the surface heat loss due to turbulent transfer, $-(E+H_\Gamma)$, and the net warming or cooling at the surface, $(Q_{VO}+S)$. These parameters are related by the following expression

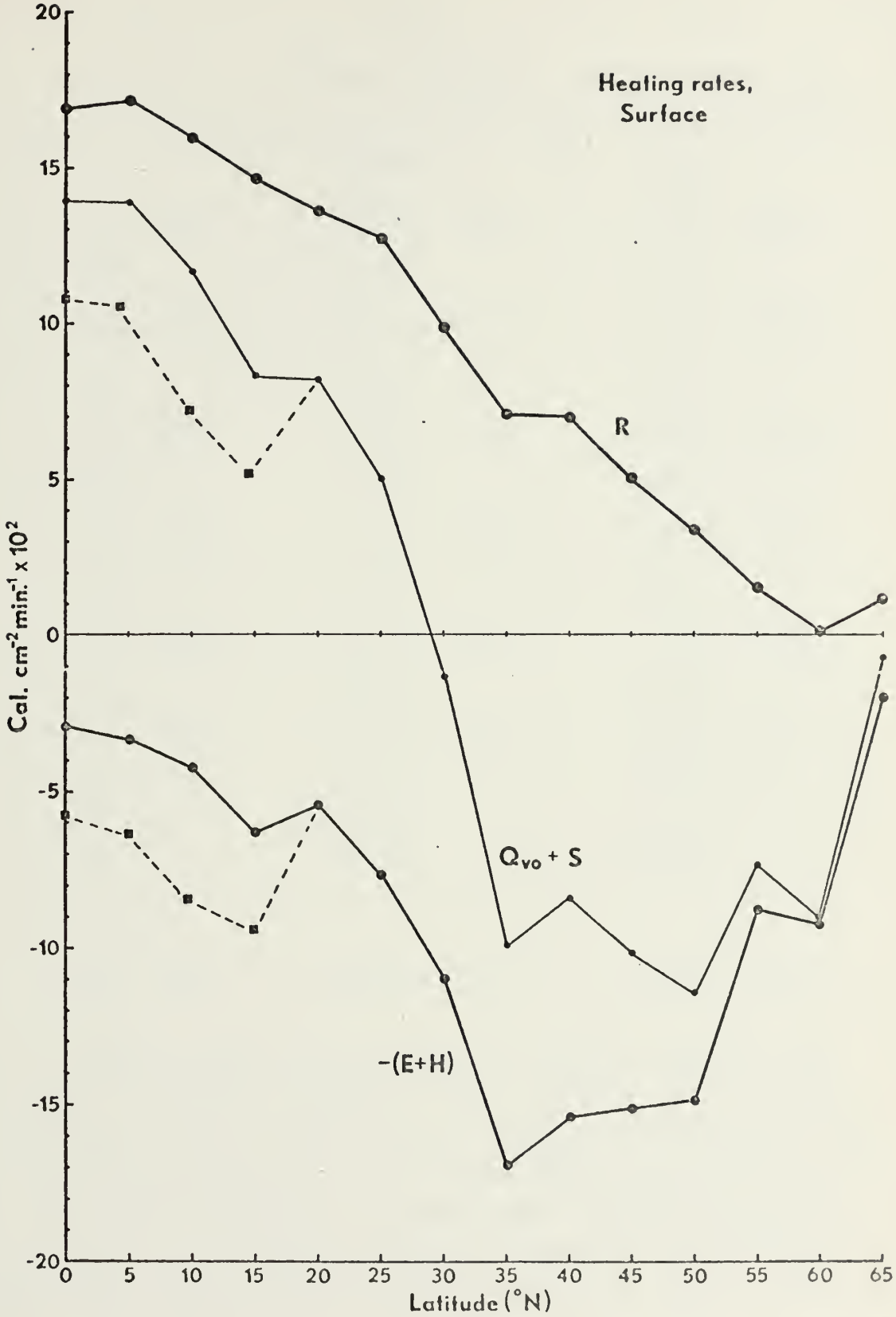

Figure 14. Surface heat budget disposition. The net warming (cooling) rate at the earth's surface (Q_{VO}+S) is given by the sum of the net radiative surface warming rate R and the loss rate due to turbulent heat transfer, -(E+H).

°LAT	(a) R_1 / R_2	(b) $-(E+H_\Gamma)_1/-(E+H_\Gamma)_2$	(c) $(Q_{VO}+S)_1/(Q_{VO}+S)_2$
0	.1687/	-.0294/	.1393/
5	.1720/.2033	-.0332/-.1539	.1388/ .0494
10	.1596/	-.0425/	.1171/
15	.1463/.2040	-.0636/-.1786	.0827/ .0304
20	.1361/	-.0544/	.0817/
25	.1276/.1900	-.0774/-.1748	.0502/ .0152
30	.0982/	-.1104/	-.0122/
35	.0705/.1482	-.1701/-.1615	-.0996/-.0133
40	.0703/	-.1544/	-.0841/
45	.0499/.1026	-.1518/-.1254	-.1019/-.0228
50	.0335/	-.1486/	-.1151/
55	.0146/.0646	-.0880/-.0988	-.0734/-.0342
60	.0013/	-.0924/	-.0911/
65N	.0120/	-.0188/	-.0068/
Wt. Avg.	.1037/.1625	-.0855/-.1533	.0182/ .0092

Table V. Comparisons of net radiative warming rate at the surface (R), the heat loss rate at the surface due to turbulent transport $-(E+H_\Gamma)$, and the net warming or cooling at the earth's surface $(Q_{VO}+S)$ for 16 October 1973 (denoted by subscript "1"). For comparison, annual mean values reported by Malkus (1962) are listed at selected latitudes (denoted by subscript "2"). All values are in ly min^{-1}.

$$Q_{vo} + S = R - (E+H_T) \qquad (7-4)$$

where S is the oceanic heat-storage term. Again it was not possible here to separate the contributions, Q_{vo} and S. The square points and dashed-in portion of the $-(E+H_T)$ and Q_{vo} curves depict the effect of varying the K* value in Eq. (5-1) as discussed in Sec. VII.C. The overall distribution in the net oceanic heating rate (Q_{vo}+S) is the same for both choices of K*. However this rate is somewhat reduced for the case of the larger K* values suggested as applicable for the tropics.

Table V shows quantitatively the difference in the parameters depicted in Fig. 14 as found by this study for 16 October 1973 and the climatological annual values reported by Malkus (1962). Note the smaller mean seasonal radiational warming rate (R) and the effect of the smaller mean heat loss by turbulent transfer in giving a slightly larger mean warming of the surface.

VIII. CONCLUSIONS

A heat budget model for inclusion in the FNWC numerical weather prediction scheme was evaluated using data along four meridional lines over the Pacific and Atlantic Oceans. These data soundings were used to compute a space-time average of the radiational and turbulent heating parameters for one day over an ocean environment. This space-time average agreed reasonably well with values derived from other studies, including satellite measurements. There were some obvious differences which could be ascribed to the seasonality of the data used in this study comprising only a one day space-time average while the comparison data was averaged over years to arrive at climatological results.

Other differences could be ascribed to the two-cloud layer parameterization for cloud amounts, the treatment of cloud reflectivity and absorptivity for solar wave lengths, and the parameterization of sensible and latent heat transfers. At this stage in the model testing, it would seem that the radiational estimates are still somewhat questionable due to the adoption of the Smagorinsky-type cloud amounts. However the regular variation of the radiative terms from gridpoint to gridpoint tends to support the apparent realism of the radiative model. The turbulent transfer heating rates of the model seem to be subject to a greater degree of possible random error due to uncertainty of the vertical gradients involved near the surface.

To complete the comparisons of the radiational aspects of this model with cited climatological data (see Sec. VII) and with satellite data, further testing should be done at different seasons of the year and possibly over other oceanic areas. Thus with a full year of representative data, refinements of the cloud-cover parameterization and in the cloud absorption and reflection values used in the model may be assessed.

Finally, the greatest gridpoint to gridpoint variability occurred in connection with the computation of evaporative and sensible heat parameters. It is perhaps here that the moisture and heating source terms used in the FNWC prediction model might best be improved.

LIST OF REFERENCES

1. Arakawa, A., 1972: Design of the UCLA General Circulation Model, Numerical Simulation of Weather and Climate Tech. Rpt. No. 7, Department of Meteorology, University of California.

2. Budyko, M.I., 1956: The Heat Balance of the Earth's Surface, Leningrad, pp. 255 (Translated by N.A. Slepanova; translation distributed by U.S. Weather Bureau, Washington, D.C.)

3. Coulson, K.L., 1959: Radiative Flux from the Top of a Rayleigh Atmosphere, Ph.D. Dissertation, Department of Meteorology, University of California, pp. 60.

4. Dixon, W.J., 1973: Biomedical Computer Programs, University of California Press, pp. 773.

5. Fleagle, R.G., Businger, J.A., 1963: An Introduction to Atmospheric Physics, Academic Press, New York, pp. 346.

6. Gates, W.L., Batten, E.S., Kahle, A.B., and Nelson, A.B., 1971: A Documentation of the Mintz-Arakawa Two-Level Atmospheric Circulation Model, Advance Research Projects Agency Report No. R-877-ARPA, Rand Corporation, Santa Monica, California, pp. 408.

7. Hanson, K.J., 1971: Studies of Cloud and Satellite Parameterization of Solar Irradiance at the Earth's Surface, paper presented at the Miami Workshop on Remote Sensing, Miami, Florida, 29-31 March 1971.

8. Jacobs, W.C., 1951: "Large-Scale Aspects of Energy Transformation over the Oceans," Compendium of Meteorology, American Meteorological Society, Boston, Mass., pp. 1103-1111.

9. Jenks, F.W., 1974: Radiative Parameterization for the FNWC Global Primitive Equation Model, M.S. Thesis, Department of Meteorology, Naval Postgraduate School, Monterey, California, pp. 89.

10. Joseph, J.H., 1971: "On the Calculation of Solar Radiation Fluxes in the Troposphere," Solar Energy, Vol. 13, Pergamon Press, London, pp. 251-261.

11. Kaitala, J.E., 1974: Heating Functions and Moisture Source Terms in the FNWC Primitive Equation Models, paper presented at the Continuing Education Program for Meteorological Specialists, Naval Postgraduate School, Monterey, California, 29 April 1974.

12. Katayama, A., 1966: "On the Radiation Budget of the Troposphere over the Northern Hemisphere (I)," Journal of the Meteorological Society of Japan, Vol. 44, No. 6, pp. 381-401.

13. Kesel, P.G., Winninghoff, F.J., 1972: "The Fleet Numerical Weather Central Operational Primitive-Equation Model," Monthly Weather Review, Vol. 100, No. 5, pp. 360-373.

14. List, R.J., 1958: Smithsonian Meteorological Tables, Smithsonian Institute, Washington, pp. 527.

15. Malkus, J.S., 1962: "Large Scale Interactions," The Sea, Vol. 1, Interscience Publishers.

16. Martin, F.L., 1972: Description of a Radiation Package for the Naval Postgraduate School General Circulation Model, Department of Meteorology, Naval Postgraduate School, Monterey, California.

17. Martin, F.L., 1974: Unpublished manuscript, Department of Meteorology, Naval Postgraduate School, Monterey, California.

18. Möller, F. and Raschke, E., 1964: Evaluation of TIROS III Radiation Data, National Aeronautics and Space Administration Contractor Rpt. NASA CR-112, Washington, D.C., pp. 114.

19. Plante, R.J., 1973: Tests of a Radiative Transfer Model for Numerical Prediction of the Atmospheric General Circulation, M.S. Thesis, Department of Meteorology, Naval Postgraduate School, Monterey, California, pp. 115.

20. Quinn, W.H., 1971: Studies of Parameterization of Solar Irradiance at the Earth's Surface, paper presented at the Miami Workshop on Remote Sensing, Miami, Florida, 29-31 March 1971.

21. Raschke, E., Vonder Haar, T., Bandeen, W., Pasternak, M., 1973: "The Annual Radiation Balance of the Earth-Atmosphere System during 1969-70 from NIMBUS III Measurements," Journal of the Atmospheric Sciences, Vol. 30, No. 3, pp. 341-364.

22. Rodgers, C.D., 1967: "The Radiative Heat Budget of the Troposphere and Lower Stratosphere," Planetary Circulation Project Report N. A2, Dept. of Meteorology, Massachusetts Institute of Technology, pp. 99.

23. Sasamori, T., 1968: "The Radiative Cooling Calculation for Application to General Circulation Experiments," Journal of Applied Meteorology, Vol. 7, No. 5, pp. 721-729.

24. Sellers, W.D., 1965: Physical Climatology, University of Chicago Press, pp. 272.

25. Smagorinsky, J., 1960: "On the Dynamical Prediction of Large Scale Condensation by Numerical Methods," Geophysical Monograph, No. 5, American Geophysical Union, Washington, D.C., pp. 71-78.

26. Smith, W.L., 1966: "Note on the Relationship Between Total Precipitable Water and Surface Dew Point," Journal of Applied Meteorology, Vol. 5, No. 5, pp. 726-727.

27. Yamamoto, G., 1952: "On a Radiation Chart," Science Repts. of the Tohoku University, Series No. 5, pp. 9-23.

INITIAL DISTRIBUTION LIST

		No. Copies
1.	Defense Documentation Center Cameron Station Alexandria, Virginia 22314	2
2.	Library, Code 0212 Naval Postgraduate School Monterey, California 93940	2
3.	Professor F. L. Martin, Code 51Mr Department of Meteorology Naval Postgraduate School Monterey, California 93940	8
4.	LT Michael D. Warner, USN 1120 West Kaler Drive Phoenix, Arizona 85021	2
5.	Department Chairman, Code 51 Department of Meteorology Naval Postgraduate School Monterey, California 93940	1
6.	Asst. Professor R. L. Haney, Code 51Hy Department of Meteorology Naval Postgraduate School Monterey, California 93940	1
7.	Naval Weather Service Command Naval Weather Service Headquarters Washington Naval Yard Washington, D. C. 20390	1
8.	Naval Oceanographic Office Library (Code 3330) Washington, D. C. 20373	1
9.	Commanding Officer Fleet Numerical Weather Central Monterey, California 93940	3
10.	Commanding Officer Environmental Prediction Research Facility Monterey, California 93940	1

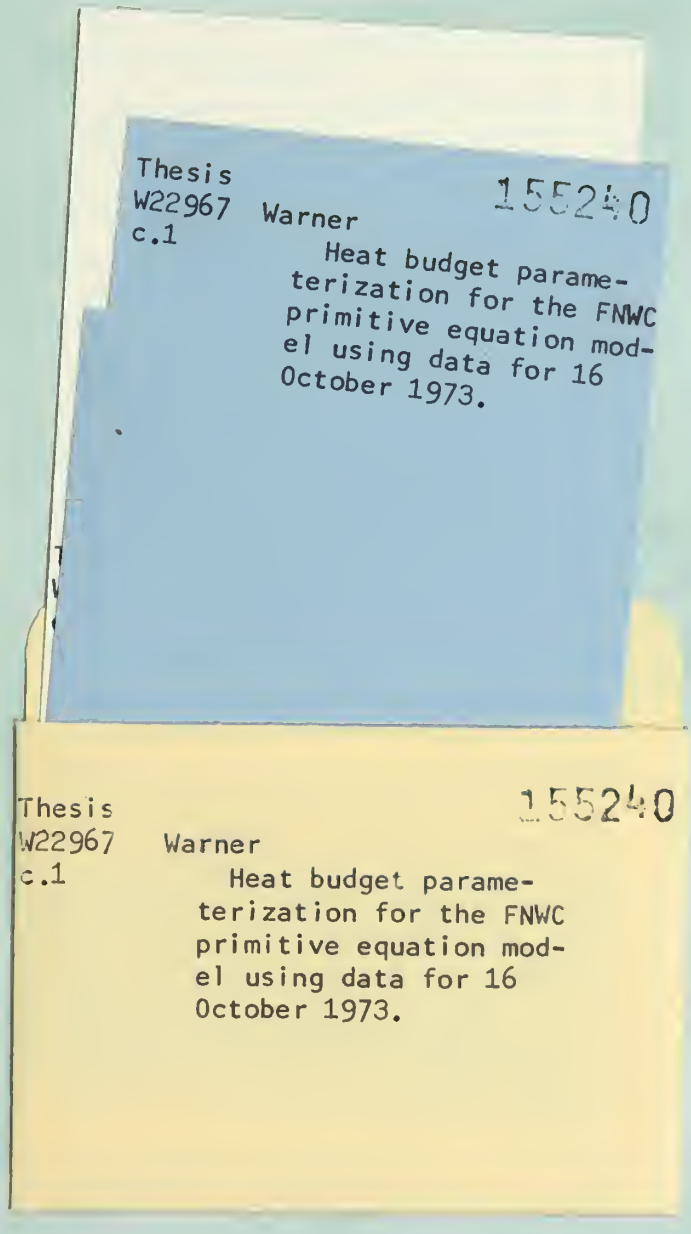

Thesis
W22967
c.1
Warner
155240
Heat budget parameterization for the FNWC primitive equation model using data for 16 October 1973.